

Crop productivity and soil inorganic carbon change mediated by enhanced rock weathering in farmland: A comparative field analysis of multi-agroclimatic regions in central China

Fuxing Guo^{a,b}, Yanping Wang^{a,b,c}, Haoyong Zhu^a, Chuangye Zhang^a, Huawei Sun^{a,d}, Zhuling Fang^a, Jing Yang^a, Linsen Zhang^e, Yan Mu^f, Yu Bon Man^g, Fuyong Wu^{a,b*}

^aCollege of Natural Resources and Environment, Northwest A&F University, Yangling 712100, Shaanxi, PR China

^bKey Laboratory of Plant Nutrition and the Agri-environment in Northwest China, Ministry of Agriculture, Yangling 712100, Shaanxi, PR China

^cFuping Modern Agricultural Comprehensive Experimental Demonstration Station, Northwest A&F University, Fuping 711700, Shaanxi, China

^d*State Key Laboratory of Soil Erosion and Dryland Farming on the Loess Plateau, Institute of Soil and Water Conservation, Chinese Academy of Sciences & Ministry of Water Resources, Yangling 712100, China*

^eCollege of Horticulture, Northwest A&F University, Yangling 712100, Shaanxi, China

^fCollege of Landscape Architecture and Arts, Northwest A&F University, Yangling 712100, Shaanxi, China

⁸Consortium on Health, Environment, Education and Research (CHEER), Department of Science and Environmental Studies, The Education University of Hong Kong, Tai Po, Hong Kong, PR China

*Corresponding author

E-mail address: wfy09@163.com (Wu Fuyong)

Abstract:

CONTEXT: Farmland enhanced rock weathering (ERW) is a negative emission technology that accelerates CO₂ sequestration into the soil inorganic carbon (SIC) sink by applying calcium and magnesium-rich silicate rock to agricultural soils. Farmland ERW has great CO₂ removal potential and is accompanied by various co-benefits, such as improving soil pH and providing mineral nutrients. However, the environment-driven mechanisms of ERW remain

29 unclear, and the uncertainty on crop productivity also requires further evaluation in field
30 trials.

31 **OBJECTIVE:** We tried to explore the response of crop productivity and soil inorganic carbon
32 to ERW in farmland and analyze the contribution and prioritization of environment drivers
33 for the above change.

34 **METHODS:** A series of monitoring trials were established in a multi-agroclimatic region in
35 central China from 2019 to 2021. Firstly, crop productivity and SIC change mediated by
36 ERW were evaluated by applying 10 kg m^{-2} mixed rock powder in field trials. Secondly, the
37 random forest and correlation network analysis were used to quantify the influence of climate,
38 soil, and management drivers on yield and SIC change. Finally, the carbon footprint of
39 silicate rock powder was calculated by life cycle analysis.

40 **RESULTS AND CONCLUSIONS:** Farmland ERW significantly improved the crop yield ($7 \pm 4.3\%$) and biomass ($11 \pm 4.6\%$) in the whole region. In the low water balance region, the
41 net carbon sequestration during three years caused by ERW was $4.31 \pm 0.82 \text{ t-CO}_2 \text{ ha}^{-1}$,
42 which increased the carbon capture of the agricultural system by 1.6-2.4 times. Contribution
43 analysis showed that soil pH had the highest relative importance (18%) on yield change
44 mediated by ERW. Low soil pH was conducive to yield and nutrient effectiveness increases,
45 and the largest yield increase reached $31 \pm 6.9\%$. Water balance (rainfall/evapotranspiration)
46 was the dominant driver affecting (20%) inorganic carbon sequestration, the accumulation of
47 SIC in low water balance reached 3.8 times that in high water balance regions. Moreover,
48 fertilizer input also significantly correlated with ERW field effect, and N input significantly
49 increased the SIC in the arid region.
50

51 **SIGNIFICANCE:** This study provided detailed field data for large-scale potential analysis of
52 ERW in farmland. These findings contribute to understanding the environmental influence of
53 ERW and assisting decision-making for ERW layout. Moreover, our results could inspire soil
54 improvement in regions with soil acidification and mineral nutrient shortages.

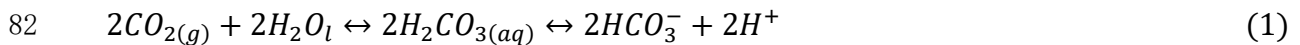
55 **Keywords:** Negative emissions technology; Enhanced silicate rock weathering; Crop
56 productivity; Soil inorganic carbon; Influence assessment.

57 **1. Introduction**

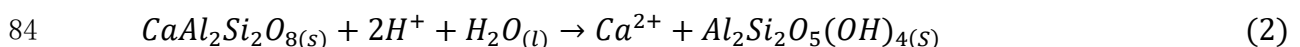
58 The severity of climate change and its associated risks have forced various sectors to act
59 to reduce greenhouse gas emissions and achieve carbon neutrality urgently (Rockström et al.,
60 2017; Notaro et al., 2022). As the world's largest user of land, agriculture systems have
61 played a vital role in such actions (Blignaut et al., 2022), contributing to global strategic
62 carbon dioxide removal (CDR) through multi-directional measures such as soil organic
63 carbon sequestration (0.5–5 gigatonnes of CO₂ per year, Gt-CO₂ yr⁻¹),
64 afforestation/reforestation (0.5–3.6 Gt-CO₂ yr⁻¹) and bio-energy with carbon capture and
65 storage (0.5–5 Gt-CO₂ yr⁻¹) (Fuss et al., 2018). However, a large gap remains between CDR
66 strategic and emission reduction targets because of the scale and cost constraints (IPCC, 2018;
67 UNEP, 2020). More collaborative CDR strategies are required to increase further the carbon
68 sequestration potential of agricultural systems.

69 The recent proposal of enhanced rock weathering (ERW) in farmland may provide a
70 new way to promote agricultural carbon sequestration (Köhler et al., 2010; Hartmann et al.,
71 2013; Beerling et al., 2020). Farmland ERW refers to the amending farmland soils with
72 artificially crushed silicate rocks to accelerate CO₂ sequestration (Köhler et al., 2010;
73 Hartmann et al., 2013). In the case of anorthite, CO₂ from atmospheric or respiration formed
74 carbonic acid through hydration, and the products were dominated by HCO₃⁻ and H⁺ in soil
75 solutions, as in eq (1) (Haque et al., 2019; Haque et al., 2020a). The weathering of exogenous
76 silicate rocks consumed H⁺, accelerates the dissolution of CO₂ in eq (1), and releases alkali
77 ions (Ca²⁺) and secondary minerals (kaolinite) as in eq (2) (Rinder and Hagke, 2021). Under
78 the further regulation of soil pH and dry and wet conditions, weathering products either form
79 secondary carbonate precipitation such as eq (3) or flow out of the soil with soil drainage and
80 into the global water systems (Berner, 2003; Penman et al., 2020).

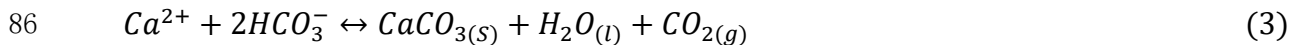
81 CO₂ dissolution:



83 Anorthite weathering:



85 Secondary carbonate precipitation:



87 The application of silicate rock powder also provided many other benefits for
88 agricultural production, such as improving soil pH (olivine) (Dietzen et al., 2018), supplying
89 potassium (K) (plauenite) (Liu et al., 2017), increasing soil phosphorus (P) effectiveness
90 (andesite) (Dalmora et al., 2020), and especially providing significant quantities available Si
91 (Jariwala et al., 2022). As a beneficial nutrient, Si was able to help crops withstand biotic and
92 abiotic stresses via forming phytoliths, reducing soil toxicity, and improving nutrient
93 effectiveness (Hartmann et al., 2013; Dalmora et al., 2020; Jariwala et al., 2022). The
94 available silicon in many farmlands, especially in acidic soils, was depleted due to repeated
95 harvesting, but the current widespread NPK fertilization schemes cannot alleviate this issue
96 (Hartmann et al., 2013; Swoboda et al., 2021). Silicate rocks occurred widely and carried a
97 wide range of mineral nutrients (e.g., Ca, Mg, K, Fe, Na), so large-scale ERW was
98 theoretically feasible and critical to addressing food security and climate change (Deer et al.,
99 2013). However, the current reports on the crop growth and nutrient supply potential of ERW
100 remain have certain contradictions. Among 61 treatments of rock powder in 40 relative
101 studies, 37 treatments significantly improved crop growth, while 24 exhibited no significant
102 changes or even had negative effects (Swoboda et al., 2021). Some negative results that were
103 not statistically significant also caused concern about the nutrient supply potential of
104 amended soil by rock powder (Priyono and Gilkes, 2008; Ramezanian et al., 2013). Moreover,
105 the weathering environment provided by farmland for silicate rock was not the same as
106 natural weathering feedback, and the interaction mechanisms between ERW and various
107 aspects of agricultural systems remain unclear. Because of single monitoring conditions and
108 short test time, current studies are difficult to clearly describe the complexity of the multiple
109 environmental factors on ERW (Rinder and Hagke, 2021; Swoboda et al., 2021). The field's
110 environmental drivers of rock weathering are also difficult to understand by inter-study
111 comparisons due to large differences in rock types, application rates, and plant and soil types
112 (Swoboda et al., 2021). Relevant experiments are therefore necessary to investigate better the

113 influence mechanism of ERW in the climate–soil–management integrated agricultural system
114 to explain the contradictions and differences in current studies.

115 In addition, the public is unaware of the seriousness of farmland soil inorganic carbon
116 (SIC) degradation and the value of ERW strategy for its restoration. SIC was traditionally
117 considered extremely stable and could be maintained for tens of thousands of years
118 (Schlesinger, 1985), so its role in the global carbon cycle and climate change was often
119 overlooked (Tao et al., 2022). However, the vulnerability of SIC in farmland was
120 significantly increased in agricultural intensification (Zamanian et al., 2018; Kim et al., 2020).
121 The losses of CaCO₃ from arable soils were substantially faster than those from natural soils
122 (Kim et al., 2020). Studies at various scales fully reported that anthropogenic activities such
123 as unreasonable N input and irrigation in intensive agricultural systems had aggravated SIC
124 loss (Dong et al., 2016; Qiu et al., 2016; Zamanian et al., 2018; Raza et al., 2020). Especially
125 in China, which consumed about 30% of the world's N fertilizer, and one of the severe
126 consequences of nitrification-induced soil acidification was the rapid loss of soil SIC (Li et
127 al., 2007; Guo et al., 2010). Tao et al (2022) reported that Chinese farmland lost 27-38% of
128 SIC and 0.53 units of soil pH in the 0-40 cm soil layer from 1980 to 2010. Song et al (2022)
129 indicated that the loss of SIC from farmland in China over the past three decades has offset
130 approximately 57% of the increase in organic carbon sequestration. Not merely sequestering
131 CO₂, SIC also plays an essential role in agricultural production by buffering soil pH,
132 activating nutrients, and stabilizing organic carbon (Wang et al., 2015; Raza et al., 2020).
133 Thus, it is urgent to seek reasonable means to improve the vulnerability of SIC to intensive
134 management. ERW introduced a silicate buffer system into the soil, alleviating soil
135 acidification and increasing soil carbonate accumulation (Dietzen et al., 2018; Haque et al.,
136 2019). The combined application of silicate rocks and fertilizers also improved the efficiency
137 of N utilization and crop yield (Blanc-Betes et al., 2020; Jariwala et al., 2022). However, the
138 impact of fertilizer and other artificial management on the field effect of slowly weathering
139 silicate rock is yet uncertain.

140 Although China has a large area of farmland and abundant silicate raw materials
141 (Beerling et al., 2020), farmland ERW remains understudied. In this study, a regional

142 evaluation of ERW was thus conducted in a multi-climate study region to (1) explore the
143 response of crop productivity and SIC to ERW applied in agricultural environments, and (2)
144 analyze the climate, soil and management drivers of subsequent ERW yield and SIC change.
145 This study aimed to provide detailed field evidence for farmland ERW to elucidate the
146 underlying mechanisms and assist decision-making.

147 **2. Materials and Methods**

148 **2.1 Description of the study area**

149 From north to south, the study area ranged from the Loess Plateau of China across the
150 Guanzhong Plain and Qinling Mountains, which includes over 8° of latitude
151 ($38^{\circ}10'70''$ – $29^{\circ}57'10''$) and within 4° of longitude ($108^{\circ}02'50''$ – $111^{\circ}86'70''$) (Fig. 1a). The
152 climate ranged widely from north to south across temperate semi-arid, subtropical monsoon
153 and subtropical plateau mountain regions with an annual average rainfall of 451.6 ± 187.4 to
154 1035 ± 321.7 mm, and average air temperatures of 8.5 ± 1.9 °C to 16.7 ± 3.9 °C. The soil
155 leaching properties varied substantially from region to region (Fig. 1b), from typical primary
156 soils (Loessial soil) in the north to semi-leached soils (Cinnamon soil, Brown soil) in the
157 middle and leached soils (Yellow-brown soil) in the south with pH values of 7.5–8.5 to
158 4.5–5.7 and base saturation > 70% to > 10%. The terrain and farmland management modes
159 were diverse as the former included plateaus, plains and mountains, while the latter included
160 ecological agriculture focused on preventing soil erosion in the Loess Plateau, intensive
161 management with high inputs and high yields in the Guanzhong Plain and extensive
162 management by scattered mountain smallholders in the Qinling Mountains (Fig. 1c, d). The
163 comparison of climate and soil characteristics in each region is shown in Fig. S1 and S2.

164 **2.2 Experiment design and sampling**

165 To promote the uniform distribution of study sites, the study area was divided into eight
166 landscape units based on climate and soil conditions (Fig. 1e). The number of study sites in
167 each landscape unit was allocated according to the area percentage. From north to south, the
168 soil types of the study sites mainly included loessial soil, cinnamon soil, brown soil and
169 yellow-brown soil, with pH between 4.7 to 8.2, and soil organic matter between 0.5 and 2.4%.

170 The soil texture was mainly sandy loam, loam and clay loam, with soil clay between 8-37%.
171 The selected fields were all bare farmland intended for long-term and exclusively agricultural
172 use. GPS receivers (Garmin eTrex 30) were used to identify the coordinates. 5 m × 5 m
173 monitoring quadrats in each field were set for ERW treatment (T_{ERW}) with 10 kg m⁻² (100 t
174 ha⁻¹) mixed silicate rock powder to improve the topsoil in April and May 2019. Mixed rock
175 powder was manually spread and incorporated into the 0-20 cm soil layer by tillage in every
176 quadrat. The mixed silicate rock powder consisted of peridotite, serpentine, diabase, plauenite,
177 andesite and basalts in a mass ratio of 1:1:1:1:5. Untreated areas in each field were used as
178 control treatments (T_C). All treatments avoided other mineral-type soil amendments (such as
179 lime) except for the mixed rock powder. Corn was planted in all study sites from May to
180 October, and winter wheat was planted in over half of the sites after the corn was harvested
181 (November to May). Field management, including tillage, nutrient input (N, P, K and organic
182 fertilizer) and irrigation were consistent in T_C and T_{ERW} at each site.

183 Yield and biomass statistics were conducted during the corn and wheat harvests (October
184 and May) each year, and soil samples were only taken in October of each year. Based on the
185 five-point sampling method (Gong, 2000; Ming, 2013), 1 m × 1 m sampling plots were set at
186 the diagonal intersection of each quadrat and four corners located 1.0 m from the boundary,
187 and all aboveground biomass in the five plots was collected to assess the differences in crop
188 growth between treatments. The plant samples were killed at 95 °C for 30 min and dried at
189 65 °C for 48 h to measure the dry weight. Yield referred to the seed's dry weight, biomass
190 was the non-seed aboveground biomass. Soil samples were taken from the centre of each
191 sampling plot with a soil drill (10 cm increments), and the 0–40 cm soil layer was collected to
192 calculate the average changes in soil depth. The reasons based on such depth are because (1)
193 fertilizers are typically applied by tillage up to 0-40 cm depth (Dong et al., 2016; Hao et al.,
194 2018), (2) crop roots are mainly distributed in such layers (Zhao et al., 2020), (3) climatic
195 factors like temperature and rainfall mainly affect the upper soil layers (Li et al., 2021; Tao et
196 al., 2022), and (4) most existing studies have focused on the SIC changes in these soil layers
197 (Li et al., 2007; Qiu et al., 2016; Tao et al., 2022).

198 2.3 Data measurement and collection

199 Table 1 shows detailed descriptions of all variables in field monitoring and
200 environmental driver data. The former included yield, biomass, SIC, soil pH, and
201 exchangeable nutrients (P, K, Ca, Mg, etc), determined by the difference between T_C and
202 T_{ERW} . The latter included climate information (radiation, temperature, rainfall,
203 evapotranspiration and water balance), initial soil parameters, such as soil texture, pH, cation
204 exchange capacity (CEC), soil carbon fraction, and management data (tillage, fertilizer and
205 irrigation).

206 2.3.1 Measurement of soil data

207 Soil sample analyses were conducted in the Key Laboratory of Plant Nutrition and the
208 Agri-environment of the Ministry of Agriculture in Northwest China. The soil particle
209 composition was determined using a laser particle sizer (Mastersizer 2000, Malvern). To
210 exclude interference from organic matter and carbonates, the 0.5 g sample was treated with
211 10 ml 15% H_2O_2 and 10 ml 0.2 mol L^{-1} HCl, respectively. Soil samples were dispersed using
212 10 ml 0.05 mol L^{-1} sodium hexametaphosphate and ultrasonic dispersion for 10 min (Arriaga
213 et al., 2006; Sochan et al., 2012). International classification standards were used to classify
214 soil particles as gravel (> 2 mm), sand (0.02-2 mm), silt (0.002-0.02 mm) and clay (< 0.002
215 mm). Soil pH was measured using an FE28 pH Meter (FE28, Mettler) calibrated with
216 standard solutions at pH 4.01 (0.05 mol L^{-1} $C_8H_5KO_4$), 6.86 (0.025 mol L^{-1} KH_2PO_4), and
217 9.18 (0.01 mol L^{-1} $Na_2B_4O_7$). Soil carbon (SOC and SIC) was measured with a combustion
218 method automatic carbon and nitrogen analyzer (Primacs SNC100, Skalar).

219 Soil exchange nutrients were measured using an inductively coupled plasma optical
220 emission spectrometer (ICP-OES; ARCOS, SPECTRO). For the macronutrients (P, K, Ca
221 Mg Si) and Al, the 5.00 g acid and neutral soils (inorganic carbon < 1.2 g kg^{-1}) were extracted
222 by 50 ml 1 mol L^{-1} ammonium acetate solution (pH = 7), centrifuged at 3600 r min^{-1} for 5
223 min, repeated for 3 times and transferred into a 250 ml volumetric flask (MoA, 2006) and the
224 5.00 g calcareous soils (inorganic carbon ≥ 1.2 g kg^{-1}) were extracted by 50 ml 10.1 mol
225 L^{-1} ammonium chloride (pH = 8.5)-ethanol solution (70%), shocked at 180 r min^{-1} for 30 min,
226 repeated 3 times, stayed overnight and transferred into a 250 ml volumetric flask (MoA,
227 2008). For micronutrients (Fe Cu, Zn, Mn), DTPA-CaCl₂-TEA (pH = 7.3) was used as an

228 extractant (MoA, 2004), 10.00 g soil was mixed with 20 ml extractant and shocked for 2 h at
229 180 r min⁻¹. Each soil sample was repeated four times in all analysis, and the maximum
230 relative error (MRE) and relative standard deviation (RSD) were less than 5.0%. The
231 calibration and calculation for ICP-OES were added in Table S2.

232 2.3.2 Collection of climate and management data

233 Meteorological datasets were collected from the National Meteorological Information
234 Center (NMIC, 2017), Resource and Environment Science and Data Center (Xu, 2022). The
235 Ångström–Prescott equation (Allen et al., 1998) was used to convert sunshine hours to solar
236 radiation as follows:

237
$$H = H_L \times \left(a + b \times \frac{S}{S_L} \right) \quad (1)$$

238 where H is the daily solar radiation (MJ m^{-2}); H_L is the daily solar radiation in sunny
239 conditions; S and S_L represent the sunshine hours and day lengths, respectively; and a and b
240 are empirical parameters with values ranging from 0.16 to 0.20 and 0.43 to 0.58, respectively.
241 For detailed calculations, see the Supplementary Materials.

242 The evapotranspiration of each site was calculated based on the FAO-PM model (Allen
243 et al., 1998):

244
$$ET_0 = \frac{0.408\Delta(R_n - G) + \gamma(900/(T + 273))u_2(e_s - e_a)}{\Delta + \gamma(1 + 0.34u_2)} \quad (2)$$

245 where ET_0 is potential evapotranspiration; Δ denotes the slope of the vapor pressure curve
246 ($\text{kPa } ^\circ\text{C}^{-1}$); R_n is the net radiation ($\text{MJ m}^{-2} \text{ d}^{-1}$); G is the soil heat flux density ($\text{MJ m}^{-2} \text{ d}^{-1}$); γ
247 denotes the psychrometric constant ($\text{kPa } ^\circ\text{C}^{-1}$); T is the daily mean air temperature ($^\circ\text{C}$); and
248 u_2 is the average daily wind speed at a 2-m height (m s^{-1}). The quadrat management data
249 were obtained by surveying the administrators or farmers, which included fertilizer (N, P, K
250 and organic fertilizer) input and irrigation.

251 2.4 Sources and characteristics of silicate rock

252 The rock source was determined through the processes of searching and screening.
253 Firstly, a preliminary search for rock sources was conducted within 300 km of the study area
254 using the national mineral deposits database of the National Geological Archives (NGA,

255 2019) to find ultramafic and basaltic rocks. Then, the rock source was screened according to
256 the following: (1) the maximum theoretical CO₂ capture potential (RCO₂) of rock was higher
257 than 0.1, and the RCO₂ (t-CO₂ t-rock⁻¹) was calculated (Renforth, 2012) as follow;

258
$$RCO_2 = \frac{M_{CO_2}}{100} \left(\frac{\%CaO}{M_{CaO}} + \frac{\%MgO}{M_{MgO}} \right) \cdot \omega - \frac{\%CO_2}{100} \quad (3)$$

259 where %CaO, %MgO and %CO₂ is the mass percentages of the elements in the rock (Table
260 S2); the M are the molecular masses, ω (1.7, referring to previous studies) is the additional
261 draw down from cation flux into the ocean (Kheshgi, 1995; Renforth, 2012; Amann et al.,
262 2020); (2) the trace elements (Cd, Hg, As, Pb, Cr) content of rock lower than the
263 GB15618-2018: Risk control standard for soil contamination of agricultural land (MEE,
264 2018); and (3) based on highways and national road, a rock source with the shortest
265 transportation distance was allocated for each field to reduce the transportation cost and
266 eliminate redundant rock sources (Fig. 1e and Fig. S3). Finally, 10 rock products were
267 determined, which included two ultrabasic rocks (one serpentine and one peridotite), six basic
268 rocks (five basalts and one diabase) and two intermediate rocks (one andesite and one
269 plauenite). Each rock powder was mixed in equal mass proportions and used for each study
270 site to (1) eliminate uncertainty due to differences in rock properties, (2) make rock
271 properties more general and regionally representative, and (3) make rock nutrients more
272 diverse to avoid the stress caused by a single element in excess.

273 Rocks were uniformly crushed twice (jaw and cone crusher), milled once (ball milling),
274 and passed through a 200-mesh sieve. Rock particle size was measured with the laser particle
275 sizer (Mastersizer 2000, Malvern) (Arriaga et al., 2006), and the Brunauer–Emmett–Teller
276 (BET) specific surface area was measured based on the BET N₂-adsorption method
277 (Brunauer et al., 1938) with the specific surface area and pore size distribution analyzer
278 (V-sorbx2800p, Gold APP). The average P80 (80% of particles with a diameter less than) of
279 the mixed rock powder was 38.4 ± 4.5 μm (Fig. S4), and the mean BET specific surface area
280 was 13.8 ± 2.7 m² g⁻¹. Rock powder mineral composition was measured by an X-ray
281 diffractometer (XRD, D8 ADVANCE A25, Bruker) based on the K-value method (Chung,
282 1974; NBS, 1986) (Fig. S5). The software Jade. 9 and standard card library PDF-4+2009 of

the International Centre for Diffraction Data (ICDD) was adopted to analyze crystalline mineral phases. The main minerals in the mixed rock powders were plagioclase (31.9 %) and augite (18.0%) (Table S1). The main element composition of the rock was analyzed by X-ray fluorescence (XRF, SPECTRO, MIDEX) and melting method. The trace element (Cd, Hg, As and Pb) was analyzed by microwave digestion and ICP-OES (SAMR and SAC, 2020). The inorganic carbon content in rocks was measured using the combination method automatic carbon and nitrogen analyzer (Primacs SNC100, Skalar) to remove the influence of carbonate minerals. The mean proportion of SiO₂ in mixed rock powder was 49.7%, and the mean proportion of alkaline oxides (CaO + MgO) was 17.8 % (Table S2).

2.5 Determination of carbon footprint

2.5.1 Carbon sequestration

Field carbon sequestration consisted of two parts: soil organic carbon (SOC) and SIC sequestration. Taking SIC as an example, the calculation process was displayed as follows:

$$SICS = \left(\sum_{i=1}^n [d_i \times \Delta SIC_i \times BD_i \times 10 \times (1 - G_i)] \right) \times \frac{M_{CO_2}}{M_C} - [\%CO_2 \times R_{Mix}] \quad (4)$$

where, *SICS* is the amount of soil inorganic carbon sequestration (t-CO₂ ha⁻¹); *d_i* is the depth of soil layer *i* (m); ΔSIC_i is the soil inorganic carbon change during monitoring (g kg⁻¹); *BD_i* is soil bulk density (g cm⁻³); *G_i* is the gravel content (> 2 mm); *M_{CO₂}* and *M_C* is the molecular masses of CO₂ and C; $\%CO_2$ is the mass percentages of the CO₂ in the rock; *R_{Mix}* is the application rate of mixed rock powder.

2.5.2 Carbon emission

According to the "cradle-to-gate" process required by the PAS 2050:2011 Protocol (BSI and Carbon Trust, 2011), carbon emissions were calculated using the LCA method. The system boundary was from "underground mine drilling and blasting " to " applied to farmland ". Functional units i.e. per unit weight expressed as tons CO₂-equivalents per ton of rock powder (t-CO₂ t-rock⁻¹). Carbon emissions were mainly divided into four modules; 1. mining, 2. processing, 3. transportation and distribution, and 4. application on farmland (Fig. S6),

which referred to a classic basic rock processing line flow (Renforth, 2012; Lefebvre et al., 2019). Direct carbon emissions included diesel combustion during mining and transportation, and blasting of emulsion explosives during mining. The proportion of explosives was 82% ammonium nitrate, 12% water content, and 6% liquid paraffin oil. Various greenhouse gases, such as carbon dioxide (CO_2), methane (CH_4) and nitrous oxide (N_2O) produced by blasting and combustion were all converted into CO_2 fluxes through the global warming potential (CWP) (Church et al., 2013; Kashyap and Agarwal, 2021). Indirect carbon emissions included purchased electrical energy and lubricants used in equipment maintenance. Packaging consumables of products and equipment were not counted, because they were rarely used and will be recycled by third parties. The carbon emission statistical model was built based on Python 3.8, and the datasets of emission factors and energy consumption coefficients were listed in Table S3.

2.6 Data analysis

2.6.1 Statistical analysis

The non-parametric Kruskal–Wallis test ($p < 0.05$) was performed to determine significance because it does not require normally distributed data. Pearson correlation and linear regression were used to analyze the relationship between variables. This analysis was conducted using the statsmodels (version 0.12.2) package in Python 3.8.

2.6.2 Evaluating the contributions of environmental drivers based on the random forest algorithm

Random forest (RF) is an aggregate model based on bagging integrated machine learning (Breiman, 2001; Li et al., 2021); it iteratively learns classification and regression trees to quantitatively analyze nonlinear interactions between variables (Li et al., 2021; Leroux et al., 2022). RF models have a strong anti-noise ability, are not prone to overfitting and can process high-dimensional data with many features, and the multiple decision trees are independent, which saves computing costs (Breiman, 2001; Li et al., 2021). Previous studies have shown that RF models outperform many other machine learning methods in agricultural research (Li et al., 2021).

337 In this study, the feature importance of the RF regression algorithm was used to quantify
 338 the contribution of climate, soil and management drivers on yield and SIC change caused by
 339 ERW. We optimized two hyperparameters of the RF model: the number of the trees
 340 (`n_estimators`) and the random seed (`random_state`). Grid searching was utilized to find the
 341 optimal combination of hyperparameters. Model performance was evaluated with 5-fold
 342 cross-validation. The definition range and optimal combination of hyperparameters are
 343 provided in Table S4. The RF regressor model and optimization were implemented using the
 344 scikit-learn (version 1.1.0) package in Python 3.8. The explained variance (R^2) and relative
 345 root mean square error (rRMSE) were used to evaluate model performance as follows:

$$346 \quad R^2 = \frac{\sum_{i=1}^n (x(i) - \bar{x})(y(i) - \bar{y})}{\sqrt{\sum_{i=1}^n (x(i) - \bar{x})^2} \sqrt{\sum_{i=1}^n (y(i) - \bar{y})^2}} \quad (5)$$

$$347 \quad \quad \quad RMSE \\
 348 \quad = \sqrt{\frac{\sum_{i=1}^n (x(i) - y(i))^2}{n}} \quad (6)$$

$$349 \quad \quad \quad rRMSE \\
 350 \quad = \frac{RMSE}{\bar{x}} \quad (7)$$

351 where $x(i)$ and $y(i)$ are the observed and predicted values, respectively; \bar{x} and \bar{y} denote the
 352 average observed and predicted values, respectively; and n is the number of samples.

353 2.6.3 Correlation network analysis of environmental drivers

354 As an efficient means of data mining and visual analysis, correlation network analysis
 355 can intuitively reflect the functional relationships in datasets (Leroux et al., 2022). The
 356 network is visualized as nodes representing variables and edges connecting nodes indicating
 357 the correlation coefficients (r), which reflect the magnitude of the co-linear relationships
 358 between the variables. In this study, we calculated the direct correlations of climate, soil and
 359 management drivers to yield and SIC change, as well as the indirect correlations between
 360 climate, soil and management drivers. Pearson correlation was used to calculate correlation

361 coefficients between all paired variables, and only significant correlations were shown in the
362 correlation network ($p < 0.05$).

363 3. Results

364 3.1 Response of crop growth and soil inorganic carbon to enhanced rock weathering

365 Yield and biomass statistics in Fig. 2a, d showed that enhanced rock weathering
366 treatment (T_{ERW}) significantly increased crop yield ($p < 0.05$) and biomass ($p < 0.01$). The
367 mean yield and biomass of the T_{ERW} were 7.11 ± 1.67 and 8.23 ± 2.55 t ha⁻¹, increased by $7 \pm$
368 4.3 % and 11 ± 4.6 % in the control treatment (T_c). Moreover, the yield increase in the benefit
369 of ERW was concentrated in the first two years, and the biomass increased significantly in
370 the three years (Fig. 2b, d). T_{ERW} simultaneously reduced the number of low-yielding fields
371 (Fig. 2c, f), the number of quadrats with yields less than 5 t ha⁻¹ decreased from 31% (T_c) to
372 13% (T_{ERW}), and the number of fields with biomass less than 7 t ha⁻¹ decreased from 58%
373 (T_c) to 34% (T_{ERW}).

374 The comparison results of SIC revealed that SIC occurred without significant ($p > 0.05$)
375 change across the region (Fig. 3a) during three years. Nevertheless, the interannual change
376 indicated that the SIC of TERW has increased significantly in the third year ($p < 0.05$), and
377 the frequency distribution showed that the SIC less than 2.8 g kg⁻¹ decreased from 71% (T_c)
378 to 53% (T_{ERW}) (Fig. 3b, c). The comparison results of soil pH revealed that the T_{ERW}
379 significantly ($p < 0.05$) increased soil pH (Fig. 3d, e) in three years, the mean soil pH of the
380 T_{ERW} was 7.24 ± 1.16 , increased by 0.32 ± 0.19 compared with the T_c (6.92 ± 0.98). From the
381 frequency distribution (Fig. 3f), T_{ERW} reduced the frequency of low pH (4.5-5.5) fields, and
382 the frequency of quadrats with soil pH less than 5.5 decreased from 17% (T_c) to 7% (T_{ERW}).

383 3.2 The relative contributions of environmental drivers based on the random forest model

384 The feature importance of the random forest models was used to quantify the relative
385 contribution of environmental drivers to the predictive variables (yield and SIC changes).
386 Based on the 17 factors in this study, the RF model explained 83% (relative Root Mean
387 Square Error, rRMSE= 18.3%) and 87% (rRMSE= 14.4%) of the yield and SIC changes,
388 respectively (Fig. 4a, e).

389 The dominant driver type of yield change was soil factors (38%). The initial soil pH was
390 the largest relative importance reaching 18% (Fig. 4a). Temperature and rainfall were the
391 main climate driving forces, and the relative influence was 27 and 37% in climate analysis
392 (Fig. 4b). The main management driver affecting ERW yield increase (Fig. 4c) was K (26%),
393 P (23%) and organic fertilizer (20%) inputs. The dominant driver type of SIC change was
394 climate factors (41%), and the relative impact of water balance was 20%, which is the largest
395 environmental driver (Fig. 4d). The main soil driver of affecting ERW yield increase (Fig. 4g)
396 was initial soil pH (36%). N and organic fertilizer inputs were the main management drivers,
397 and the relative influence was 36 and 31% in management analysis (Fig. 4h).

398 3.3 The partial dependence analysis of environmental drivers

399 The partial dependence analyses of impact factors further illustrate the relationship
400 between environmental drivers and predictive variables (Fig. 5 and Fig. S7). The predicted
401 yield change was negatively correlated with initial soil pH, SIC, CEC, P and K input ($p <$
402 0.01), and revealed a significant positive correlation with rainfall and organic fertilizer inputs
403 ($p < 0.001$). The predicted SIC change was negatively correlated with water balance and
404 rainfall ($p < 0.05$) and was positively correlated with initial soil pH, SIC, N and organic
405 fertilizer input ($p < 0.05$), while no significant relationship was observed with other factors.
406 Moreover, in the partial dependence analysis, the predicted yield and SIC changed most
407 obviously with initial soil pH (4.5-7.5) and water balance (0.8-1.1).

408 The influence of initial soil pH and water balance was further analyzed. Yield change
409 significantly decreased with the increasing initial pH (Fig. 6a), and the significant increase in
410 yield was concentrated at sites with initial soil pH below 6.5. The average yield of T_{ERW} (6.26
411 $\pm 1.85 \text{ t ha}^{-1}$) was increased by $16.7 \pm 5.2\%$. The yield changes also significantly decreased
412 with P and K inputs (Fig. 6b). The yield increases in site with low pH and low nutrient
413 inputing further expanded to $31 \pm 6.9\%$ (Fig. 6c). The change of SIC increased first and then
414 decreased with water balance, and was negatively correlated as a whole ($p < 0.05$), The
415 significant increase of SIC was concentrated at sites with water balance less than 0.8, and the
416 SIC significantly increased by $12.5 \pm 8.6\%$ (Fig. 6d, f). The change of SIC was not

417 significantly correlated with initial soil pH. The accumulation of SIC was mainly
418 concentrated in the pH range of 6-7.5 (Fig. 6e).

419 3.4 Carbon budget of farmland ERW in low water balance region

420 The carbon budget (Fig. 7) revealed that ERW substantially increased the carbon capture
421 in the low water balance (≤ 0.8) region. The inorganic carbon sequestration caused by ERW
422 was $4.31 \pm 0.82 \text{ t-CO}_2 \text{ ha}^{-1}$ for three years, which was similar to the organic carbon
423 sequestration ($4.43 \pm 1.32 \text{ t-CO}_2 \text{ ha}^{-1}$). The net carbon sequestration of T_{ERW} was 7.12 ± 1.87
424 $\text{t-CO}_2 \text{ ha}^{-1}$, $101 \pm 38.4\%$ higher than that of T_C ($3.54 \pm 0.68 \text{ t-CO}_2 \text{ ha}^{-1}$). The total carbon
425 emissions from T_{ERW} was $1.57 \pm 0.34 \text{ t-CO}_2 \text{ ha}^{-1}$, which accounted for $36.4 \pm 7.8\%$ of the
426 inorganic carbon sequestration. Moreover, processing and transport were the main emission
427 processes, accounting for 43 and 37% of the total emissions, respectively.

428 The combined carbon sequestration potential of ERW with conventional tillage (CT) and
429 conservation agriculture (CA) was further explored. The combined carbon sequestration of
430 CT and ERW ($7.16 \pm 1.83 \text{ t-CO}_2 \text{ ha}^{-1}$) was 2.5 times higher than that of the CT system (2.83
431 $\pm 0.46 \text{ t-CO}_2 \text{ ha}^{-1}$), and 1.5 times higher than that of CA system ($4.65 \pm 1.26 \text{ t-CO}_2 \text{ ha}^{-1}$). The
432 combined CA and ERW had the highest carbon sequestration potential ($8.01 \pm 2.26 \text{ t-CO}_2$
433 ha^{-1}), $72 \pm 18.4\%$ higher than that of the CA system and $12 \pm 6.9\%$ higher than that of the
434 CT+ERW system.

435 3.5 The correlation network analysis of environmental drivers

436 The correlation network analysis revealed that the significant relationship between
437 environmental drivers and yield, SIC changes were based on low initial soil pH and low
438 water balance (Fig. 8). The initial soil pH exhibited the strongest negative correlation ($r =$
439 -0.62 , $p < 0.01$) with yield change in the whole regional (Fig. 8a), but other correlation
440 coefficients between factors and yield changes were all lower than 0.4. In the low soil pH (\leq
441 6.5) region (Fig. 8b), the correlation between each factor and yield change was substantially
442 enhanced, and the correlation coefficients of rainfall, initial CEC, initial SIC, P input and K
443 input with yield changes were 0.53 , -0.58 , -0.51 , -0.67 and -0.70 ($p < 0.05$), respectively. In
444 high soil pH (> 6.5) region (Fig. 8c), the yield change was only significantly correlated with

445 organic fertilizer inputs ($r = 0.29, p < 0.01$), initial CEC ($r = -0.36, p < 0.001$) and initial SIC
446 ($r = -0.23, p < 0.01$).

447 In the whole regional analysis (Fig. 8d), the correlation coefficient between SIC change
448 and water balance was $-0.74 (p < 0.01)$, while the correlation with other drivers was all lower
449 than 0.35. In the low water balance (≤ 1.1) region (Fig. 8e), the correlation coefficient
450 between SIC change and rainfall ($r = 0.47, p < 0.001$), initial soil pH ($r = -0.51, p < 0.001$),
451 CEC ($r = -0.64, p < 0.001$), N input ($r = 0.62, p < 0.001$) and organic fertilizer input ($r = 0.41,$
452 $p < 0.001$) increased rapidly. In the high-water balance (> 1.1) region (Fig. 8f), SIC change,
453 however, was only significantly correlated with N input ($r = 0.26, p < 0.05$), organic fertilizer
454 input ($r = 0.34, p < 0.01$), and soil clay ($r = 0.31, p < 0.05$). Correlation coefficient matrices
455 were supplemented in Fig. S8.

456 3.6 Relationship between soil carbon components and SIC change

457 The relationship between SIC change induced by ERW and other soil carbon
458 components was further explored (Fig. 9). Total soil carbon change exhibited a significantly
459 ($p < 0.01$) positive relationship with SIC change (Fig. 9a), and no significant relationship was
460 observed between SOC and SIC change (Fig. 9b). It can be seen that ERW increased total
461 soil carbon sequestration potential by improving SIC accumulation, and did not reduce SOC
462 storage. However, the correlation analysis showed that the initial SOC content and the
463 organic fertilizer input were significantly positively correlated with the change of SIC (Fig.
464 9c, d), indicating that the transformation of organic carbon components may be beneficial to
465 the accumulation of SIC. Furthermore, the soil water-soluble organic carbon and microbial
466 organic carbon also showed a significant positive correlation with SIC change under the
467 condition of low water balance (Fig. 9e, f).

468 3.7 Effects of enhanced rock weathering on soil exchange nutrients

469 The comparison results of soil exchange nutrients are shown in Fig. 10. T_{ERW}
470 demonstrated prominent multi-nutrient benefits in the whole region, and the contents of soil
471 exchange P, Ca Mg and Si in T_{ERW} were significantly ($p < 0.05$) higher than those in Tc.
472 Furthermore, the multi-nutrient benefits of ERW were also regulated by initial soil pH. In low

473 soil pH sites, the benefits of multi-nutrients were more substantial, soil exchange P, K, Ca,
474 Mg, Fe and Si of T_{ERW} all increased significantly ($p < 0.05$), while only soil exchange Mg and
475 Si increased significantly ($p < 0.05$) in high soil pH sites. Moreover, the soil exchange Al in
476 low soil pH sites decreased significantly ($p < 0.001$), reflecting the potential of T_{ERW} to
477 alleviate Al toxicity.

478 **4. Discussion**

479 4.1 The effect of enhanced rock weathering on crop productivity

480 4.1.1 Enhanced rock weathering contributes to improved yield on a large scale.

481 One of the most attractive aspects of ERW was its yield increase effect. The evidence
482 presented in this study indicated that the ERW based on mixed rock powder had significantly
483 improved the crop yield ($7 \pm 4.3\%$) and aboveground biomass ($11 \pm 4.6\%$) of farmland at
484 the regional scale ([Fig. 2](#)). This result supported the view of relevant studies (Hartmann et al.,
485 2013; Beerling et al., 2018; Kelland et al., 2020) that amending farmland soil through basic
486 and ultrabasic rocks contributed to alleviating the food security crisis in a large-scale as a
487 result of improvements in soil nutrient availability (Silva et al., 2014; Shah et al., 2018) and
488 crop metabolic activity and stress resistance (Crusciol et al., 2019; Li et al., 2020). Due to the
489 randomness and diversity of the field environment, the yield gain of this study was slightly
490 lower than the results of controlled environmental trials. For instance, sorghum yield
491 increased by 21% following the amendment of a neutral clay loam ($\text{pH} = 6.6$) with basalt (10
492 kg m^{-2}) without P and K input ([Kelland et al., 2020](#)), durum wheat grain yield increased by
493 18.4% under improved neutral soil ($\text{pH} = 6.0$) with glauconite (0.2 kg m^{-2}) ([Rudmin et al.,
494 2019](#)), and ryegrass biomass increased by 15.6% under improved acid sandy soil ($\text{pH} = 4.9$)
495 with olivine ($0.16\text{-}20.4 \text{ kg m}^{-2}$) ([ten Berge et al., 2012](#)). Silicate rock powder has been
496 particularly prominent in improving the growth of leguminous crops. For example, green
497 bean yield gain was 64% in neutral ($\text{pH} = 6.63$) sandy loam with wollastonite (7.5 kg m^{-2})
498 ([Jariwala et al., 2022](#)), and the soybean yield increased by two-fold amended with 10 kg m^{-2}
499 wollastonite ([Haque et al., 2020b](#)). A substantial biomass accumulation increase of beans
500 reported by Haque et al (2019) reached 177% in acid soil ($\text{pH} = 4.9$) modified by high-load

501 wollastonite (221 t ha^{-1}). It can be seen that ERW could play a more attractive role in
502 increasing crop productivity in the context of more targeted soil or crops. However, it is
503 worth noting that ERW was required a reasonable application rate and rock quality.
504 Otherwise, it may cause nutrient imbalance (Priyono and Gilkes, 2008) or the accumulation
505 of toxic elements (ten Berge et al., 2012; de Souza et al., 2018).

506 4.1.2 Initial soil pH is the key environment driver

507 Under the premise of controlling the rock type and particle size, the analysis of this study
508 revealed that the initial soil pH played a crucial role in the ERW-mediated yield change.
509 Initial soil pH had the highest relative contribution (18%), and yield change exhibited
510 significant ($p < 0.01$) negative correction with soil pH (Fig. 4a and Fig. 5a). The yield
511 improvement effect in the low soil pH was $16.7 \pm 5.2\%$, which was 2.4 times higher than that
512 in the whole region (Fig. 6a, c). The previous review also put forward a similar view: most of
513 the current significant yield increase experiments occurred in acidic (mainly oxidized) soil
514 (Swoboda et al., 2021). Soil pH can control plant nutrient availability by mediating the ability
515 of soil to absorb and temporarily retain nutrients (Malik et al., 2018; Haque et al., 2019), and
516 the range of 5-8.5 was beneficial for cultivation (Jariwala et al., 2022). In acidic, especially in
517 strongly acidic soil, the enriched H^+ and Al^{3+} displaced significant amounts of nutrients from
518 inorganic and organic ligands into the soil solution, thereby accelerating the loss of available
519 nutrients (Guo et al., 2010; Strefler et al., 2018; Raza et al., 2020). If the soil pH was less than
520 5, Al could cause toxicity to plant roots, nutrient uptake and leaf photosynthesis rates were
521 reduced by more than 30% (Guo et al., 2010; Wang et al., 2015). Silicate minerals could
522 consume H^+ and release alkalinity during weathering, which contributed to improving soil pH
523 and reducing Al toxicity (Hartmann et al., 2013; Beerling et al., 2018; Kelland et al., 2020).
524 In this study, the addition of mixed rock powder significantly increased the soil pH (Fig. 3)
525 and decreased the soil exchangeable (ammonium acetate as leaching solution) Al (Fig. 10);
526 this result supported that the ERW strategy had the potential to replace the agricultural lime
527 currently used in large areas to improve soil acidification.

528 Moreover, the contribution analysis results showed that the input of P (14%) and K (12%)
529 also affected the yield change caused by ERW (Fig. 4a). The P and K input exhibited a

530 significant negative correlation with the yield change in low input range (Fig. 6), which
531 indicated that ERW also played an ideal role in yield increases through replacing partly
532 conventional fertilizer in the areas with insufficient P, K resources. Based on acid soil, low P
533 and K input further increased the yield improvement effect by $31 \pm 6.9\%$, which was 4.4
534 times higher than that in the whole region. The comparison results of soil exchangeable
535 nutrients also proved that ERW improved the P and K effectiveness in low pH regions (Fig.
536 10), which may be due to the more release of elements and the improvement of soil chemical
537 environment in low pH soil (Beerling et al., 2018; Swoboda et al., 2021). Although the
538 nutrient supply potential of ERW was controlled by the elements and structure in different
539 rock, almost all basic and ultrabasic rocks can indirectly improve nutrient effectiveness by
540 increased soil pH and competitive Si ions content (Dias et al., 2018; Swoboda et al., 2021).
541 Moreover, the ERW strategy was undisputed in improving soil available Si in this study (Fig.
542 10), and Si effectiveness in all types of soil increased significantly ($p < 0.01$). As a health
543 nutrient, Si has a positive significance for most conventional crops, such as rice, wheat, corn
544 and soybean. Especially for rice, the importance of Si was considered second only to N, P
545 and K (Swoboda et al., 2021). Si is the main element of building plant cell walls and plays a
546 vital role in improving crop quality, photosynthesis and stress resistance (Parr and Sullivan,
547 2010; Li et al., 2018). Due to the higher irrigation and lower soil pH, the application of rock
548 powder to the rice system may achieve a win-win situation between yield increase and carbon
549 capture in the future.

550 4.2 The effect of enhanced rock weathering on soil inorganic carbon

551 4.2.1 An efficient CDR synergy strategy by alleviating farmland SIC degradation

552 Silicate rock powder can naturally consume CO₂ in the atmosphere while weathering and
553 releasing nutrients in farmland (Zamanian et al., 2016). This carbon capture process is
554 without other pollutants either in the generation or application stage, so it is very clean and
555 has no environmental severe adverse effects when applied on a large scale (Lefebvre et al.,
556 2019). Carbon budget (Fig. 7) in low water balance region indicated that the SIC
557 sequestration of T_{ERW} was 4.31 ± 0.82 t-CO₂ ha⁻¹ within 3 years, which was similar to the
558 basalt carbon capture estimated by Kelland et al (2020) (3 t-CO₂ ha⁻¹ within 2 years).

Moreover, the carbon emission of rock powder was 1.57 ± 0.34 t-CO₂ ha⁻¹, which was only 36% of the inorganic carbon capture. Due to the different trial preconditions (rock dosage, particle size, Ca, Mg content, etc.) and statistical methods, the sequestration potential that ERW can refer to varies greatly (Table S5). Taking area as the base unit, the carbon sequestration was between 0.023 to 39.3 (median: 1.69) t-CO₂ ha⁻¹, taking rock dosage as the base unit, the carbon sequestration was between 0.10×10^{-3} to 0.31 (median: 0.07) t-CO₂ t-rock⁻¹. Further analysis showed that ERW-mediated SIC changes without led to a significant reduction in SOC. On the contrary, the input and transformation of SOC could accelerate the accumulation of SIC (Fig. 9). The increase of organic fertilizer input and active components of organic carbon (DOC, MBC) contributed to the accumulation of SIC in the low water balance zone. Previous relevant experiments had also shown that the combined application of rock powder and organic materials (such as compost and manure) had gratifying synergistic benefits, such as reducing NH₃ volatilization (Shah et al., 2018), K release (de Souza et al., 2018) and SIC accumulation (Manning et al., 2013).

The accumulation of SIC mainly occurred in semi-arid and semi-humid regions with water balance of less than 0.8 (Fig. 6d). Under this hydrological condition, the soil system lacked sufficient downward water flux or surface runoff to carry the weathering products away from the topsoil in farmland with low slope (Beaulieu et al., 2011; Tao et al., 2022). Therefore, weathering products accumulated in the topsoil layer and accelerated the formation of SIC (Zamanian et al., 2016; Dang et al., 2022). If the rock powders can be incorporated into agricultural standardization management and continue to be input to improve the soil pH in such regions, the generated SIC was theoretically stable and not decomposed or lost in the short-term, and could be considered an effective way of soil carbon sequestration. However, this view requires to be proved through long-term monitoring. In addition, the dissolution and leaching of SIC did not mean that CO₂ was released again. If viewed over a long geological time scale, the CO₂ capture by SIC was only a baseline in high water balance region, the carbon sequestration would double with the dissolution as the dissolved inorganic carbon (DIC), and eventually be converted into marine carbon sequestration as the continental water system entered rivers or oceans (Renforth, 2012;

588 Renforth and Henderson, 2017; Strefler et al., 2018; Haque et al., 2020a). However, these
589 parts were difficult to monitor in the field, and it was difficult to estimate the stability and
590 persistence of DIC in soil water solution because it may be transformed into other forms at
591 any time through adsorption, precipitation or utilization by plants and microorganisms
592 (Zamanian et al., 2016). Due to the slow weathering of the mixed rock powder used in this
593 study, the current result was only a snapshot of the ERW strategy, far from reaching the final
594 effect of ERW. Furthermore, as a continuous and clean pathway of carbon sequestration, rock
595 powder has considerable long-term benefits and will continue to play a role in crop growth
596 and agricultural systems SIC capture in the coming years. The theoretical sequestration
597 potential of rock powder could reach 16-32 t ha⁻¹ (Table S1), which was 3.7-7.4 times the
598 currently measured SIC sequestration, while the carbon emission in the rock production
599 process was only 6.9-13.8% of this theoretical sequestration potential ([Fig. 7](#)).

600 4.2.2 The accumulation of SIC is restricted by water balance

601 The release of Mg is a vital indicator for evaluating the rate of rock weathering because it
602 was less affected by plant absorption and secondary precipitation than Ca and Si (Kelland et
603 al., 2020). The Mg release rate of mixed rock powder was calculated based on the soil
604 exchangeable pool was between 10^{-14.5} to 10⁻¹², the average is 10^{-13.3±0.5}. These values were
605 similar to the Mg dissolution rates (10^{-11.8} -10^{-13.7}) of basic (basalt) and ultrabasic (olivine)
606 rock particles in mesoscale experiments (Renforth et al., 2015; Amann et al., 2020; Kelland et
607 al., 2020). Furthermore, Mg released rate exhibited a significant ($p < 0.05$) positive correction
608 with soil pH change ([Fig. S9](#)), which showed that rock weathering and the alkali ions release
609 could directly contribute to the increase in soil pH (Dietzen et al., 2018; Haque et al., 2019).
610 However, Mg released rate and pH changes failed to display a significant positive correlation
611 with SIC accumulation ([Fig. S9](#)). In low pH soils, the released alkali ions may be used to
612 exchange acidogenic ions in the soil exchange pool (ten Berge et al., 2012; Dietzen et al.,
613 2018), or they may be dissolved in the aqueous phase and infiltrate with rainwater (Renforth
614 and Henderson, 2017; Cipolla et al., 2021), so the amount of alkali ions used for secondary
615 carbonate accumulation was controlled by multiple factors such as CEC, salt base saturation

616 and soil hydrology (Maher, 2010; Zamanian et al., 2016; Zeng et al., 2022), and was not only
617 positively related to the ion release rate.

618 Due to the stringent generation conditions of SIC, the significant accumulation of SIC
619 has been reported rarely in current studies (ten Berge et al., 2012; Hartmann et al., 2013;
620 Manning et al., 2013; Haque et al., 2019; Amann et al., 2020; Haque et al., 2020a). It is
621 conservatively estimated that only when the soil pH value exceeds 6.5 is conducive to the
622 accumulation of SIC (Haque et al., 2019), even if the pCO₂ of root zone soil can be several
623 ten times higher than that of soil surface due to soil respiration and decomposition of humus
624 (Manning et al., 2013; Penman et al., 2020). Therefore, it is difficult to obtain positive results
625 from short-term (planting crops only once) trials in acid soil with low application rates or
626 large particle sizes (ten Berge et al., 2012; Dietzen et al., 2018; Amann et al., 2020). This
627 study revealed that the accumulation of SIC may be further driven by the soil water balance
628 based on satisfying the soil pH. Water balance is an effective indicator to evaluate soil
629 leaching, which can explain soil parameter variability related to leaching in a large range,
630 such as soil pH, base saturation, etc. (Yang et al., 2005; Tao et al., 2022). In the present study,
631 water balance has the highest relative importance (20%) in the change of SIC ([Fig. 4e](#)), and
632 the SIC accumulation in the low water balance was increased by $12.5 \pm 5.7\%$, which was 3.8
633 times higher than that in the high water balance region ([Fig. 6d, f](#)).

634 The large amount of N and organic matter input provided additional active H⁺ for
635 farmland soil (Zamanian et al., 2018; Raza et al., 2020). These additional active H⁺ not only
636 caused soil acidification and in-situ SIC dissolution but also reduced the dependence of the
637 rock powder weathering process on initial soil pH, and further accelerated the release of Ca²⁺
638 and Mg²⁺ from silicate minerals in neutral and alkaline soils (Monger et al., 2015; Koester et
639 al., 2021). In such cases, whether the weathering products can be further stored and
640 accumulated on the soil surface becomes critical to the formation of SIC. Therefore, the
641 significant accumulation of SIC in this study was not in the high-water balance (> 0.8) region
642 most suitable for rock weathering, which had higher rainfall, temperature and lower soil pH,
643 etc., but was concentrated in the water balance between 0.4 and 0.8 ([Fig. 6d](#)). The drastically
644 increase in the correlation between N input and SIC accumulation in the region of balance

water < 0.8 also proved this inference (Fig. 8d, e). Tao et al. (2022) also reported that the soil acidification caused by N input accelerated the silicate weathering and farmland SIC accumulation in China's arid and semi-arid regions from 1980-2010.

In the current controlled environment trials, the water supply of the containers was often larger than the evapotranspiration (that is, the water balance was relatively larger) to obtain sufficient water flow and extract for analysis in the experiments. In this hydrological environment, the highly mobile base ions may move downward with the longitudinal flow, which was not conducive to the accumulation of SIC on the surface. For example, the ratio of simulated rainfall to evapotranspiration (rough calculation based on the difference between rainfall and leakage) in the olivine mesoscopic trial reached 1.57 (Amann et al., 2020). The total irrigation amount for 120 days was 13.9 L column⁻¹ (equivalent to 766 mm) in the basic rock dust-amended experience (Kelland et al., 2020). In contrast to laboratory conditions, the reports of field experiments were positive. In the field investigation of artificial silicate weathering, it was observed that the rapid formation of carbonate "hardpan" in the soil formed by waste slag and mineral substances (Hartmann et al., 2013). Some field comparative trials also reported a significant accumulation of SIC, but the field environment was complex and lacked accurate hydrological parameters for further analysis and comparison (Manning et al., 2013; Haque et al., 2019; Haque et al., 2020a).

5. Conclusion

The complexity of multi-source driver control in the field makes it difficult to quantify the impact of ERW on agricultural systems accurately. This study analyzed the environmental drivers of ERW-mediated crop productivity, and SIC changes in a multi-agroclimatic region. Contribution analysis indicated that soil pH and water balance drove the yield and SIC change. ERW could promote food security in soil acidification and barren mineral nutrients regions with improved soil pH and nutrient effectiveness. The farmland ERW strategy was also an efficient CDR synergy strategy. The accumulation of SIC in farmland offset the carbon emissions of rock powder in production and increased the carbon sequestration by $101 \pm 38.4\%$. The current status of lime input, mineral nutrient scarcity, and water balance was recommended as a vital basis for the future deployment of

674 large-scale ERW strategies, and the layout of ERW in regions with severe soil acidification
675 and SIC degradation will also make the effect of yield and carbon sequestration more
676 attractive. Further long-term monitoring experiments are required to assess the impact of
677 ERW on soil water systems, especially dissolved inorganic carbon, to develop a more
678 comprehensive understanding of the carbon sequestration potential mediated by ERW.
679 Moreover, farmland management factors, especially fertilization, have a non-negligible
680 impact on ERW, and further experiments are required to find direct evidence to quantify this
681 impact to serve large-scale evaluation studies.

682 **Acknowledgement**

683 The financial support from the National Natural Science Foundation of China (grant
684 numbers 42077325, 41571218, 41401613) and Committee on Research and Development,
685 The Education University of Hong Kong (RG 47/2021-2022R) was gratefully acknowledged.
686 Thanks to Fuping, Mizhi, Ansai, and other experimental demonstration stations for providing
687 and managing the quadrats. Thanks to National Meteorological Information Center and
688 Resource and Environment Science and Data Center for the provision of climate data. We
689 were also sincerely grateful to the three anonymous reviewers for their corrections and
690 comments on the manuscript's methodology.

691 **Reference**

- 692 Allen, R.G., Pereira, L.S., Raes, D., Smith, M., 1998. Crop evapotranspiration-Guidelines for
693 computing crop water requirements. FAO Irrigation and drainage paper 56 300(9). FAO,
694 Rome, Italia, pp. D05109.
- 695 Amann, T., Hartmann, J., Struyf, E., Garcia, W.d.O., Schoelynck, J., 2020. Enhanced Weathering and
696 related element fluxes-a cropland mesocosm approach Biogeosciences 17.
697 <https://doi.org/10.5194/bg-17-103-2020>.
- 698 Arriaga, F.J., Lowery, B., Mays, M.D., 2006. A fast method for determining soil particle size
699 distribution using a laser instrument. Soil Sci 171, 663-674.
700 <https://doi.org/10.1097/01.ss.0000228056.92839.88>.

- 701 Beaulieu, E., Goddéris, Y., Labat, D., Roelandt, C., Calmels, D., Gaillardet, J., 2011. Modeling of
702 water-rock interaction in the Mackenzie basin: Competition between sulfuric and carbonic
703 acids. *Chem. Geol.* 289, 114-123. <https://doi.org/10.1016/j.chemgeo.2011.07.020>.
- 704 Beerling, D.J., Kantzas, E.P., Lomas, M.R., Wade, P., Eufrasio, R.M., Renforth, P., Sarkar, B.,
705 Andrews, M.G., James, R.H., Pearce, C.R., Mercure, J.F., Pollitt, H., Holden, P.B., Edwards,
706 N.R., Khanna, M., Koh, L., Quegan, S., Pidgeon, N.F., Janssens, I.A., Hansen, J., Banwart,
707 S.A., 2020. Potential for large-scale CO₂ removal via enhanced rock weathering with
708 croplands. *Nature* 583, 242-248. <https://doi.org/10.1038/s41586-020-2448-9>.
- 709 Beerling, D.J., Leake, J.R., Long, S.P., Scholes, J.D., Ton, J., Nelson, P.N., Bird, M., Kantzas, E.,
710 Taylor, L.L., Sarkar, B., Kelland, M., DeLucia, E., Kantola, I., Müller, C., Rau, G., Hansen, J.,
711 2018. Farming with crops and rocks to address global climate, food and soil security. *Nat.*
712 *Plants* 4, 138-147. <https://doi.org/10.1038/s41477-018-0108-y>.
- 713 Berner, R.A., 2003. The long-term carbon cycle, fossil fuels and atmospheric composition. *Nature*
714 426, 323-326. <https://doi.org/10.1038/nature02131>.
- 715 Blanc-Betes, E., Kantola, I.B., Gomez-Casanovas, N., Hartman, M.D., Parton, W.J., Lewis, A.L.,
716 Beerling, D.J., DeLucia, E.H., 2020. In silico assessment of the potential of basalt
717 amendments to reduce N₂O emissions from bioenergy crops. *GCB Bioenergy* 13, 224-241.
718 <https://doi.org/10.1111/gcbb.12757>.
- 719 Blignaut, J., Meissner, H., Smith, H., du Toit, L., 2022. An integrative bio-physical approach to
720 determine the greenhouse gas emissions and carbon sinks of a cow and her offspring in a beef
721 cattle operation: A system dynamics approach. *Agric. Syst.* 195, 103286.
722 <https://doi.org/10.1016/j.agsy.2021.103286>.
- 723 Breiman, L., 2001. Random forests. *Mach. Learn.* 45, 5–32. <https://doi.org/10.1023/a:1010933404324>.
- 724 Brunauer, S., Emmett, P.H., Teller, E., 1938. Adsorption of gases in multimolecular layers. *J. Am*
725 *Chem. Soc* 60, 309–319. <https://doi.org/10.1021/ja01269a023>.
- 726 BSI, Carbon Trust, 2011. Specification for the Assessment of the Life Cycle Greenhouse Gas
727 Emissions of Goods and Services. p. 36. Publicly Available Specification-PAS 2050:2011.
728 London, UK http://www.vizea.fr/actualites/6_PAS_2050.pdf.
- 729 Chung, F.H., 1974. A New X-Ray Diffraction Method for Quantitative Multicomponent Analysis.
730 *Advances in X-Ray Analysis* 17, 106-115. <https://doi.org/10.1154/s0376030800005231>.

- 731 Church, J., Clark, P., Cazenave, A., Gregory, J., Unnikrishnan, A., 2013. Climate Change 2013: The
732 Physical Science Basis. Contribution of Working Group I to the Fifth Assessment Report of
733 the Intergovernmental Panel on Climate Change. In: Stocker, T.F., Qin, D., Plattner, G.-K.,
734 Tignor, M., Allen, S.K., Boschung, J., Nauels, A., Xia, Y., Bex, V., Midgley, P.M. (Eds.),
735 Capital dilemma: Growth and inequity in Washington D.C. Cambridge University Press,
736 United Kingdom and New York, NY, USA. [https://doi.org/10.1016/S0925-7721\(01\)00003-7](https://doi.org/10.1016/S0925-7721(01)00003-7)
- 737 Cipolla, G., Calabrese, S., Noto, L.V., Porporato, A., 2021. The role of hydrology on enhanced
738 weathering for carbon sequestration I. Modeling rock-dissolution reactions coupled to plant,
739 soil moisture, and carbon dynamics. *Adv. Water Resour.* 154, 103934.
740 <https://doi.org/10.1016/j.advwatres.2021.103934>.
- 741 Crusciol, C.A.C., Moretti, L.G., Bossolani, J.W., Moreira, A., Micheri, P.H., Rossi, R., 2019. Can
742 dunite promote physiological changes, magnesium nutrition and increased corn grain yield?
743 *Commun. Soil Sci. Plant Anal.* 50, 2343–2353.
744 <https://doi.org/10.1080/00103624.2019.1659304>.
- 745 Dalmora, A.C., Ramos, C.G., Silva Oliveira, M.L., Silva Oliveira, L.F., Homrich Schneider, I.A.,
746 Kautzmann, R.M., 2020. Application of andesite rock as a clean source of fertilizer for
747 eucalyptus crop: Evidence of sustainability. *J. Clean. Prod.* 256, 120432.
748 <https://doi.org/10.1016/j.jclepro.2020.120432>.
- 749 Dang, C., Kong, F., Li, Y., Jiang, Z., Xi, M., 2022. Soil inorganic carbon dynamic change mediated
750 by anthropogenic activities: An integrated study using meta-analysis and random forest model.
751 *Sci Total Environ* 835, 155463. <https://doi.org/10.1016/j.scitotenv.2022.155463>.
- 752 de Souza, M.E.P., Cardoso, I.M., de Carvalho, A.M.X., Lopes, A.P., Jucksch, I., Janssen, A., 2018.
753 Rock powder can improve vermicompost chemical properties and plant nutrition: an on-farm
754 experiment. *Commun.Soil Sci. Plant Anal.* 49, 1–12.
755 <https://doi.org/10.1080/00103624.2017.1418372>.
- 756 Deer, W.A., Howie, R.A., Zussman, J., 2013. An Introduction to the Rock-forming Minerals. 3rd ed.
757 The Mineralogical Society, London.
- 758 Dias, K., Guimarães, P.T.G., do Carmo, D.L., Reis, T.H.P., Lacerda, J., 2018. Alternative sources of
759 potassium in coffee plants for better soil fertility, productivity, and beverage quality. *Pesq. Agrop. Brasileira* 53, 1355–1362. <https://doi.org/10.1590/s0100-204x2018001200008>.

- 761 Dietzen, C., Harrison, R., Michelsen-Correa, S., 2018. Effectiveness of enhanced mineral weathering
762 as a carbon sequestration tool and alternative to agricultural lime: An incubation experiment.
763 Int. J. Greenh. Gas Con 74, 251-258. <https://doi.org/10.1016/j.ijggc.2018.05.007>.
- 764 Dong, W., Duan, Y., Wang, Y., Hu, C., 2016. Reassessing carbon sequestration in the North China
765 Plain via addition of nitrogen. Sci Total Environ 563-564, 138-144.
766 <https://doi.org/10.1016/j.scitotenv.2016.04.115>.
- 767 Fuss, S., Lamb, W.F., Callaghan, M.W., Hilaire, J., Creutzig, F., Amann, T., Beringer, T., de Oliveira
768 Garcia, W., Hartmann, J., Khanna, T., Luderer, G., Nemet, G.F., Rogelj, J., Smith, P., Vicente,
769 J.L.V., Wilcox, J., del Mar Zamora Dominguez, M., Minx, J.C., 2018. Negative
770 emissions—Part 2: Costs, potentials and side effects. Environ. Res. Lett 13, 063002.
771 <https://doi.org/10.1088/1748-9326/aabf9f>.
- 772 Gong, J.Y., 2000. Statistical Methods for Experiment. Beijing, China Agriculture Press.
- 773 Guo, J.H., Liu, X.J., Zhang, Y., Shen, J.L., Han, W.X., Zhang, W.F., Zhang, F.S., 2010. Significant
774 acidification in major Chinese Croplands. Science 327.
775 <https://doi.org/10.1126/science.1182570>.
- 776 Hao, T., Zhu, Q., Zeng, M., Shen, J., Shi, X., Liu, X., Zhang, F., de Vries, W., 2018. Quantification of
777 the contribution of nitrogen fertilization and crop harvesting to soil acidification in a
778 wheat-maize double cropping system. Plant Soil 434, 167-184.
779 <https://doi.org/10.1007/s11104-018-3760-0>.
- 780 Haque, F., Santos, R.M., Chiang, Y.W., 2020a. CO₂ sequestration by wollastonite-amended
781 agricultural soils – an Ontario field study. Int. J. Greenh. Gas Con 97, 103017.
782 <https://doi.org/10.1016/j.ijggc.2020.103017>.
- 783 Haque, F., Santos, R.M., Chiang, Y.W., 2020b. Optimizing Inorganic Carbon Sequestration and Crop
784 Yield With Wollastonite Soil Amendment in a Microplot Study. Front Plant Sci 11, 1012.
785 <https://doi.org/10.3389/fpls.2020.01012>.
- 786 Haque, F., Santos, R.M., Dutta, A., Thimmanagari, M., Chiang, Y.W., 2019. Co-benefits of
787 wollastonite weathering in agriculture: CO₂ sequestration and promoted plant growth. ACS
788 Omega 4, 1425–1433. <https://doi.org/10.1021/acsomega.8b02477>.
- 789 Hartmann, J., West, A.J., Renforth, P., Köhler, P., Rocha, C.L.D.L., Wolf-Gladrow, D.A., Dürr, H.H.,
790 Scheffran, J., 2013. Enhanced chemical weathering as a geoengineering strategy to reduce

- 791 atmospheric carbon dioxide, supply nutrients, and mitigate ocean acidification. *Rev Geophys*
792 51, 113-149. <https://doi.org/10.1002/rog.20004>.
- 793 IPCC, 2018. Global Warming of 1.5 °C. An IPCC Special Report on the Impacts of Global Warming
794 of 1.5 °C above Pre-Industrial Levels and Related Global Greenhouse Gas Emission
795 Pathways: World Meteorological Organization. <https://www.ipcc.ch/sr15/>.
- 796 Jariwala, H., Haque, F., Vanderburgt, S., Santos, R.M., Chiang, Y.W., 2022.
797 Mineral-Soil-Plant-Nutrient Synergisms of Enhanced Weathering for Agriculture: Short-Term
798 Investigations Using Fast-Weathering Wollastonite Skarn. *Front Plant Sci* 13, 929457.
799 <https://doi.org/10.3389/fpls.2022.929457>.
- 800 Kashyap, D., Agarwal, T., 2021. Carbon footprint and water footprint of rice and wheat production in
801 Punjab, India. *Agric. Syst* 186, 102959. <https://doi.org/10.1016/j.agsy.2020.102959>.
- 802 Kelland, M.E., Wade, P.W., Lewis, A.L., Taylor, L.L., Sarkar, B., Andrews, M.G., Lomas, M.R.,
803 Cotton, T.E.A., Kemp, S.J., James, R.H., Pearce, C.R., Hartley, S.E., Hodson, M.E., Leake,
804 J.R., Banwart, S.A., Beerling, D.J., 2020. Increased yield and CO₂ sequestration potential
805 with the C₄ cereal Sorghum bicolor cultivated in basaltic rock dust-amended agricultural soil.
806 *Glob. Chang. Biol* 26, 3658-3676. <https://doi.org/10.1111/gcb.15089>.
- 807 Kheshgi, H.S., 1995. Sequestering atmospheric carbon dioxide by increasing ocean alkalinity. *Energy*
808 20, 915-922. [https://doi.org/10.1016/0360-5442\(95\)00035-f](https://doi.org/10.1016/0360-5442(95)00035-f).
- 809 Kim, J.H., Jobbagy, E.G., Richter, D.D., Trumbore, S.E., Jackson, R.B., 2020. Agricultural
810 acceleration of soil carbonate weathering. *Glob Chang Biol* 26, 5988-6002.
811 <https://doi.org/10.1111/gcb.15207>.
- 812 Koester, M., Stock, S.C., Nájera, F., Abdallah, K., Gorbushina, A., Prietzel, J., Matus, F., Klysubun,
813 W., Boy, J., Kuzyakov, Y., Dippold, M.A., Spielvogel, S., 2021. From rock eating to
814 vegetarian ecosystems — Disentangling processes of phosphorus acquisition across biomes.
815 *Geoderma* 388, 114827. <https://doi.org/10.1016/j.geoderma.2020.114827>.
- 816 Köhler, P., Hartmann, J., Wolf-Gladrow, D.A., 2010. Geoengineering potential of artificially
817 enhanced silicate weathering of olivine. *Proc. Natl Acad. Sci* 107, 20228-20233.
818 <https://doi.org/10.1073/pnas.1000545107>.
- 819 Lefebvre, D., Goglio, P., Williams, A., Manning, D.A.C., de Azevedo, A.C., Bergmann, M.,
820 Meersmans, J., Smith, P., 2019. Assessing the potential of soil carbonation and enhanced

- weathering through Life Cycle Assessment: A case study for Sao Paulo State, Brazil. *J. Clean. Prod* 233, 468-481. <https://doi.org/10.1016/j.jclepro.2019.06.099>.
- Leroux, L., Faye, N.F., Jahel, C., Falconnier, G.N., Diouf, A.A., Ndao, B., Tiaw, I., Senghor, Y., Kanfany, G., Balde, A., Dieye, M., Sirdey, N., Loison, S.A., Corbeels, M., Baudron, F., Bouquet, E., 2022. Exploring the agricultural landscape diversity-food security nexus: an analysis in two contrasted parklands of Central Senegal. *Agric. Syst* 196, 103312. <https://doi.org/10.1016/j.agsy.2021.103312>.
- Li, J., Mavrodi, D.V., Dong, Y., 2020. Effect of rock dust-amended compost on the soil properties, soil microbial activity, and fruit production in an apple orchard from the Jiangsu province of China. *Arch. Agron. Soil Sci* 16, 1–14. <https://doi.org/10.1080/03650340.2020.1795136>.
- Li, L., Wang, B., Feng, P., Wang, H., He, Q., Wang, Y., Liu, D.L., Li, Y., He, J., Feng, H., Yang, G., Yu, Q., 2021. Crop yield forecasting and associated optimum lead time analysis based on multi-source environmental data across China. *Agric. For. Meteorol* 308-309, 108558. <https://doi.org/10.1016/j.agrformet.2021.108558>.
- Li, Z., Song, Z., Yan, Z., Hao, Q., Song, A., Liu, L., Yang, X., Xia, S., Liang, Y., 2018. Silicon enhancement of estimated plant biomass carbon accumulation under abiotic and biotic stresses. A meta-analysis. *Agron Sustain Dev* 38. <https://doi.org/10.1007/s13593-018-0496-4>.
- Li, Z.P., Han, F.X., Su, Y., Zhang, T.L., Sun, B., Monts, D.L., Plodinec, M.J., 2007. Assessment of soil organic and carbonate carbon storage in China. *Geoderma* 138, 119-126. <https://doi.org/10.1016/j.geoderma.2006.11.007>.
- Liu, S., Qi, X., Han, C., Liu, J., Sheng, X., Li, H., Luo, A., Li, J., 2017. Novel nano-submicron mineral-based soil conditioner for sustainable agricultural development. *J. Clean. Prod* 149, 896-903. <https://doi.org/10.1016/j.jclepro.2017.02.155>.
- Maher, K., 2010. The dependence of chemical weathering rates on fluid residence time. *Earth Planet. Sc. Lett* 294, 101-110. <https://doi.org/10.1016/j.epsl.2010.03.010>.
- Malik, A.A., Puissant, J., Buckeridge, K.M., Goodall, T., Jehmlich, N., Chowdhury, S., Gweon, H.S., Peyton, J.M., Mason, K.E., van Agtmaal, M., Blaud, A., Clark, I.M., Whitaker, J., Pywell, R.F., Ostle, N., Gleixner, G., Griffiths, R.I., 2018. Land use driven change in soil pH affects microbial carbon cycling processes. *Nat. Commun* 9, 3591. <https://doi.org/10.1038/s41467-018-05980-1>.

- 851 Manning, D.A.C., Renforth, P., Lopez-Capel, E., Robertson, S., Ghazireh, N., 2013. Carbonate
852 precipitation in artificial soils produced from basaltic quarry fines and composts: An
853 opportunity for passive carbon sequestration. Int. J. Greenh. Gas Con 17, 309-317.
854 <https://doi.org/10.1016/j.ijggc.2013.05.012>.
- 855 MEE, 2018. GB 15618-2018: Risk control standard for soil contamination of agricultural land.
856 Ministry of Ecology and Environment of the People's Republic of China.
857 <https://www.mee.gov.cn/ywgz/fgbz/bz/bzwb/trhj/201807/W020190626595212456114.pdf>.
- 858 Ming, D.X., 2013. Field experiment and statistical analysis. Beijing, Science Press.
- 859 MoA, 2004. NY/T 890-2004: Determination of available zinc, manganese, iron, copper in
860 soil—extraction with buffered DTPA solution. Ministry of Agriculture of the PRC, China
861 Standards Press.
- 862 MoA, 2006. NY/T 1121.13-2006: Soil Testing Part 13: Method for determination of soil
863 exchangeable calcium and magnesium. Ministry of Agriculture of the PRC, China Standards
864 Press.
- 865 MoA, 2008. NY/T 1615-2008: Determination of exchangeable bases and total exchangeable bases in
866 calcareous soil. Ministry of Agriculture of the PRC, China Standards Press.
- 867 Monger, H.C., Kraimer, R.A., Khresat, S.e., Cole, D.R., Wang, X., Wang, J., 2015. Sequestration of
868 inorganic carbon in soil and groundwater. Geology 43, 375-378.
869 <https://doi.org/10.1130/g36449.1>.
- 870 NBS, 1986. GB/T 5225—1985: Metal materials—Quantitative phase analysis—"Value K" method
871 of X-ray diffraction. National Bureau of Standards of the People's Republic of China.
- 872 NGA, 2019. China Mineralogical Database 2020 Edition. National geological archives (NGA).
873 <http://data.ngac.org.cn/mineralresource/index.html?id=302c137ee126465095b3df8e68168d8c>
874 .
- 875 NMIC, 2017. China Meteorological Administration Land Surface Data Assimilation System
876 (CLDAS-V2.0) near real-time product dataset. National Meteorological Information Center
877 <http://data.cma.cn/>.
- 878 Notaro, M., Gary, C., Le Coq, J.-F., Metay, A., Rapidel, B., 2022. How to increase the joint provision
879 of ecosystem services by agricultural systems. Evidence from coffee-based agroforestry
880 systems. Agric. Syst 196, 103332. <https://doi.org/10.1016/j.agrsy.2021.103332>.

- 881 Parr, J.F., Sullivan, L.A., 2010. Phytolith occluded carbon and silica variability in wheat cultivars.
882 Plant Soil 342, 165-171. <https://doi.org/10.1007/s11104-010-0680-z>.
- 883 Penman, D.E., Rugenstein, J.K.C., Ibarra, D.E., Winnick, M.J., 2020. Silicate weathering as a
884 feedback and forcing in Earth's climate and carbon cycle. Earth-Sci. Rev 209, 103298.
885 <https://doi.org/10.1016/j.earscirev.2020.103298>.
- 886 Priyono, J., Gilkes, R.J., 2008. High-energy milling improves the effectiveness of silicate rock
887 fertilizers: a glasshouse assessment. Commun. Soil Sci. Plant Anal 39, 358–369.
888 <https://doi.org/10.1080/00103620701826498>.
- 889 Qiu, S., Gao, H., Zhu, P., Hou, Y., Zhao, S., Rong, X., Zhang, Y., He, P., Christie, P., Zhou, W., 2016.
890 Changes in soil carbon and nitrogen pools in a Mollisol after long-term fallow or application
891 of chemical fertilizers, straw or manures. Soil Till. Res 163, 255-265.
892 <https://doi.org/10.1016/j.still.2016.07.002>.
- 893 Ramezanian, A., Dahlin, A.S., Campbell, C.D., Hillier, S., Mannerstedt-Fogelfors, B., Öborn, I., 2013.
894 Addition of a volcanic rockdust to soils has no observable effects on plant yield and nutrient
895 status or on soil microbial activity. Plant Soil 367, 419–436.
896 <https://doi.org/10.1007/s11104-012-1474-2>.
- 897 Raza, S., Miao, N., Wang, P., Ju, X., Chen, Z., Zhou, J., Kuzyakov, Y., 2020. Dramatic loss of
898 inorganic carbon by nitrogen-induced soil acidification in Chinese croplands. Glob Chang
899 Biol 26, 3738-3751. <https://doi.org/10.1111/gcb.15101>.
- 900 Renforth, P., 2012. The potential of enhanced weathering in the UK. Int. J. Greenh. Gas Con 10,
901 229-243. <https://doi.org/10.1016/j.ijggc.2012.06.011>.
- 902 Renforth, P., Henderson, G., 2017. Assessing ocean alkalinity for carbon sequestration. Rev. Geophys
903 55, 636-674. <https://doi.org/10.1002/2016RG000533>.
- 904 Renforth, P., Pogge von Strandmann, P.A.E., Henderson, G.M., 2015. The dissolution of olivine
905 added to soil: Implications for enhanced weathering. Applied Geochemistry 61, 109-118.
906 <https://doi.org/10.1016/j.apgeochem.2015.05.016>.
- 907 Rinder, T., Hagke, C.v., 2021. The influence of particle size on the potential of enhanced basalt
908 weathering for carbon dioxide removal - Insights from a regional assessment. J. Clean. Prod
909 315, 128178. <https://doi.org/10.1016/j.jclepro.2021.128178>.

- 910 Rockström, J., Gaffney, O., Rogelj, J., Meinshausen, M., Nakicenovic, N., Schellnhuber, H.J., 2017.
911 A roadmap for rapid decarbonisation. Science 355, 1269–1271.
912 <https://doi.org/10.1126/science.aah3443>.
- 913 Rudmin, M., Banerjee, S., Makarov, B., Mazurov, A., Ruban, A., Oskina, Y., Tolkachev, O., Buyakov,
914 A., Shalybin, M., 2019. An investigation of plant growth by the addition of glauconitic
915 fertilizer. Appl. Clay Sci 180. <https://doi.org/10.1016/j.clay.2019.105178>.
- 916 SAMR, SAC, 2020. GB/T 6730.81-2020: Iron ores—Determination of multiple trace
917 elements—Inductively coupled plasma mass spectrometric method. State Administration for
918 Market Regulation and Standardization Administration of the People's Republic of China.
- 919 Schlesinger, W.H., 1985. The formation of caliche in soils of the Mojave Desert, California. Geochim.
920 Cosmochim. Acta 49, 57–66. [https://doi.org/10.1016/0016-7037\(85\)90191-7](https://doi.org/10.1016/0016-7037(85)90191-7).
- 921 Shah, G.A., Shah, G.M., Rashid, M.I., Groot, J.C.J., Traore, B., Lantinga, E.A., 2018. Bedding
922 additives reduce ammonia emission and improve crop N uptake after soil application of solid
923 cattle manure. J Environ Manage 209, 195–204.
924 <https://doi.org/10.1016/j.jenvman.2017.12.035>.
- 925 Silva, D.R.G., Carlos, R.S., Giuliano, M., Danilo, d., Eduardo, L.C., de. Yield, d.S.M., 2014. Yield,
926 nutrient uptake and potassium use efficiency in rice fertilized with crushed rocks. Afr. J.
927 Agric. Res 9, 455–464. <https://doi.org/10.5897/ajar2013.7638>.
- 928 Sochan, A., Bieganowski, A., Ryżak, M., Dobrowolski, R., Bartmiński, P., 2012. Comparison of soil
929 texture determined by two dispersion units of Mastersizer 2000. Inst. Agrophysics 26, 99–102.
930 <https://doi.org/10.2478/v10247-012-0015-9>.
- 931 Song, X.D., Yang, F., Wu, H.Y., Zhang, J., Li, D.C., Liu, F., Zhao, Y.G., Yang, J.L., Ju, B., Cai, C.F.,
932 Huang, B., Long, H.Y., Lu, Y., Sui, Y.Y., Wang, Q.B., Wu, K.N., Zhang, F.R., Zhang, M.K.,
933 Shi, Z., Ma, W.Z., Xin, G., Qi, Z.P., Chang, Q.R., Ci, E., Yuan, D.G., Zhang, Y.Z., Bai, J.P.,
934 Chen, J.Y., Chen, J., Chen, Y.J., Dong, Y.Z., Han, C.L., Li, L., Liu, L.M., Pan, J.J., Song,
935 F.P., Sun, F.J., Wang, D.F., Wang, T.W., Wei, X.H., Wu, H.Q., Zhao, X., Zhou, Q., Zhang,
936 G.L., 2022. Significant loss of soil inorganic carbon at the continental scale. Natl Sci Rev 9,
937 nwab120. <https://doi.org/10.1093/nsr/nwab120>.

- 938 Strefler, J., Amann, T., Bauer, N., Kriegler, E., Hartmann, J., 2018. Potential and costs of carbon
939 dioxide removal by enhanced weathering of rocks. Environmental Research Letters 13.
940 <https://doi.org/10.1088/1748-9326/aaa9c4>.
- 941 Swoboda, P., Döring, T.F., Hamer, M., 2021. Remineralizing soils? The agricultural usage of silicate
942 rock powders: A review. Sci. Total Environ. 2021, 150976.
943 <https://doi.org/10.1016/j.scitotenv.2021.150976>.
- 944 Tao, J., Raza, S., Zhao, M., Cui, J., Wang, P., Sui, Y., Zamanian, K., Kuzyakov, Y., Xu, M., Chen, Z.,
945 Zhou, J., 2022. Vulnerability and driving factors of soil inorganic carbon stocks in Chinese
946 croplands. Sci Total Environ 825, 154087. <https://doi.org/10.1016/j.scitotenv.2022.154087>.
- 947 ten Berge, H.F.M., Hugo G, v.d.M., Johan W, S., Paul W, G., Knops, P., Verhagen, J., 2012. Olivine
948 Weathering in Soil, and Its Effects on Growth and Nutrient Uptake in Ryegrass
949 (Loliumperenne L.): A Pot Experiment. PLoS ONE 7, e42098.
950 <https://doi.org/10.1371/journal.pone.0042098>.
- 951 UNEP, 2020. Emissions Gap Report 2020: United Nations Environment Programme. Nairobi.
952 <https://www.unep.org/emissions-gap-report-2020>.
- 953 Wang, C., Li, W., Yang, Z., Chen, Y., Shao, W., Ji, J., 2015. An invisible soil acidification: Critical
954 role of soil carbonate and its impact on heavy metal bioavailability. Sci Rep 5, 12735.
955 <https://doi.org/10.1038/srep12735>.
- 956 Xu, X., 2022. Annual spatial interpolation dataset of meteorological elements in China. Resource and
957 Environmental Science Data Registration and Publishing System
958 <http://www.resdc.cn/10.12078/2022082501>.
- 959 Yang, J., Ding, Y., Chen, R., Liu, L., 2005. Fluctuations of the Semi-Arid Zone in China, and
960 Consequences for Society. Clim. Chang. 72, 171-188.
961 <https://doi.org/10.1007/s10584-005-6858-3>.
- 962 Zamanian, K., Pustovoytov, K., Kuzyakov, Y., 2016. Pedogenic carbonates: Forms and formation
963 processes. Earth-Sci. Rev 157, 1-17. <https://doi.org/10.1016/j.earscirev.2016.03.003>.
- 964 Zamanian, K., Zarebanadkouki, M., Kuzyakov, Y., 2018. Nitrogen fertilization raises CO₂ efflux from
965 inorganic carbon: A global assessment. Glob Chang Biol 24, 2810-2817.
966 <https://doi.org/10.1111/gcb.14148>.

967 Zeng, S., Liu, Z., Groves, C., 2022. Large-scale CO₂ removal by enhanced carbonate weathering from
968 changes in land-use practices. Earth-Science Reviews 225, 103915.
969 <https://doi.org/10.1016/j.earscirev.2021.103915>.

970 Zhao, Q.Y., Xu, S.J., Zhang, W.S., Zhang, Z., Yao, Z., Chen, X.P., Zou, C.Q., 2020. Identifying key
971 drivers for geospatial variation of grain micronutrient concentrations in major maize
972 production regions of China. Environ Pollut 266, 115114.
973 <https://doi.org/10.1016/j.envpol.2020.115114>.

974

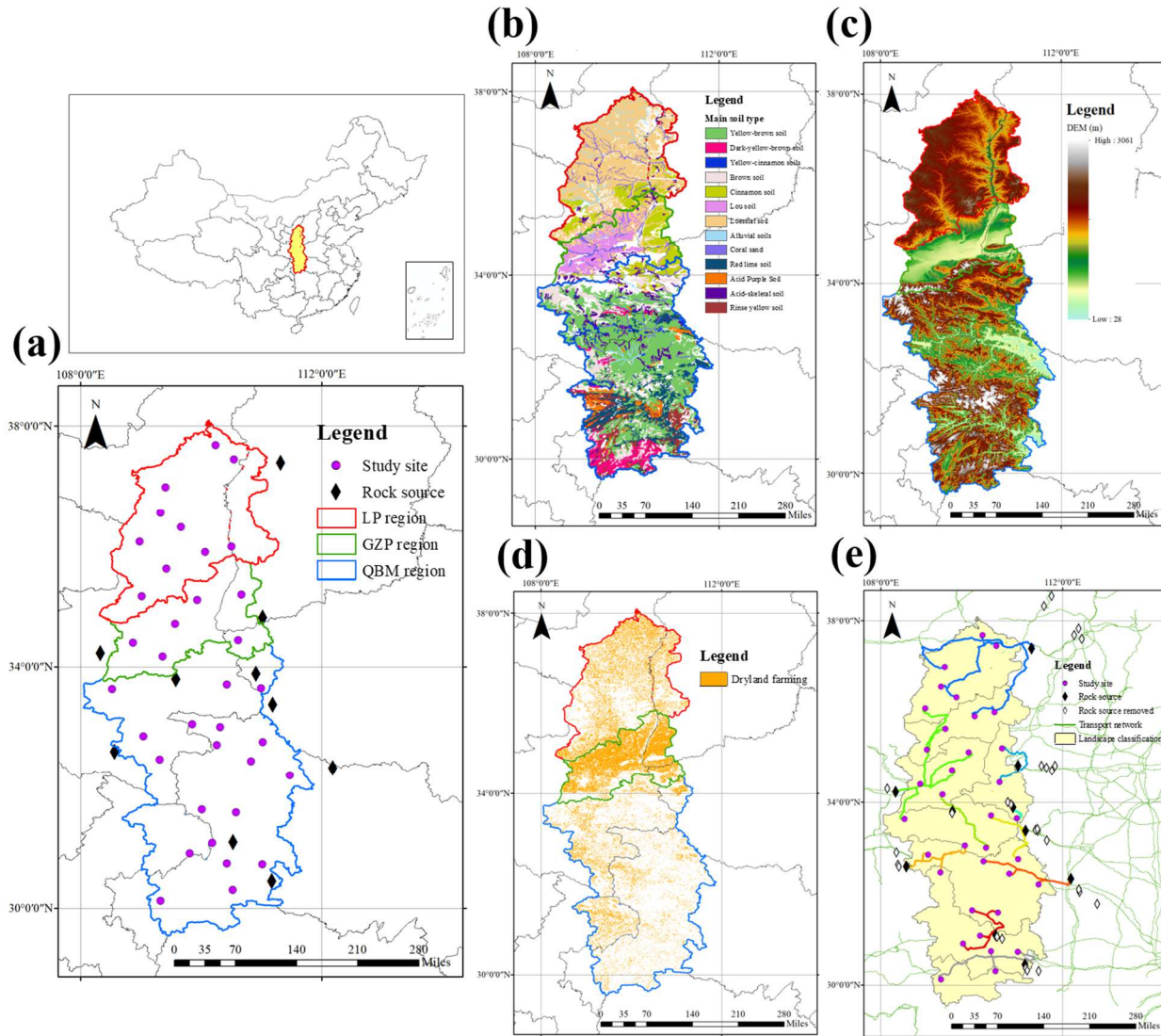


Fig. 1. Location and sample of the study area (a), and its soil type (b), elevation (DEM) (c), dryland distribution (d), and landscape classification and shortest path analysis of rock source (e). LP, GZP and QBM denote Loess Plateau region, Guan-Zhong Plain region, Qin-Ba Mountainous region, respectively.

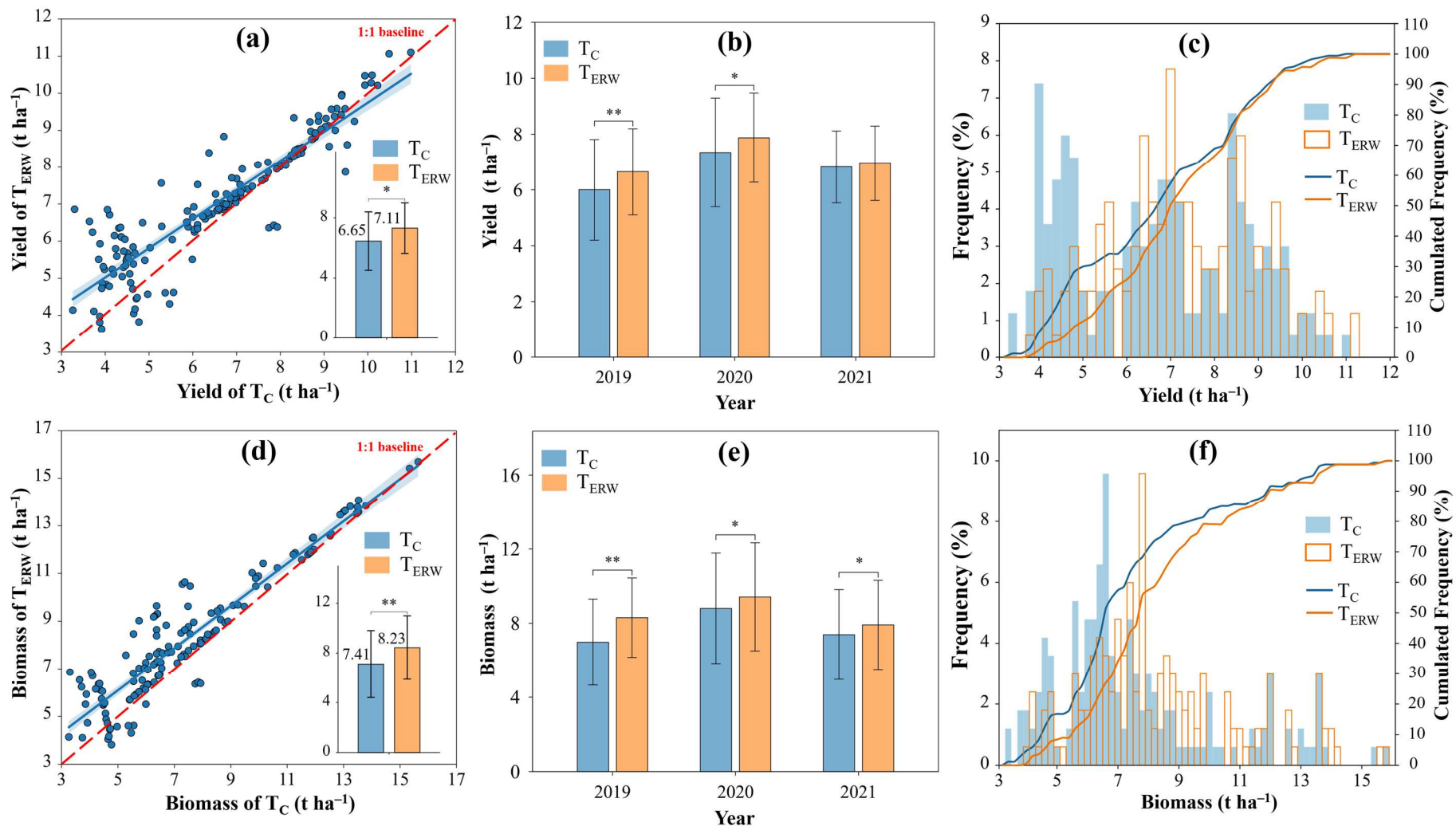


Fig. 2. The significance comparison (a, d), annual change (b, e), and frequency distribution (c, f) of yield and biomass in response to enhanced rock weathering. T_C and T_{ERW} is control and enhanced rock weathering treatment. The interior bar plot is a significant comparison in subfigure a and d, and bars show frequency and lines denote cumulated frequency in subfigure c and f. * denote $p < 0.05$, ** is $p < 0.01$, and *** represent $p < 0.001$.

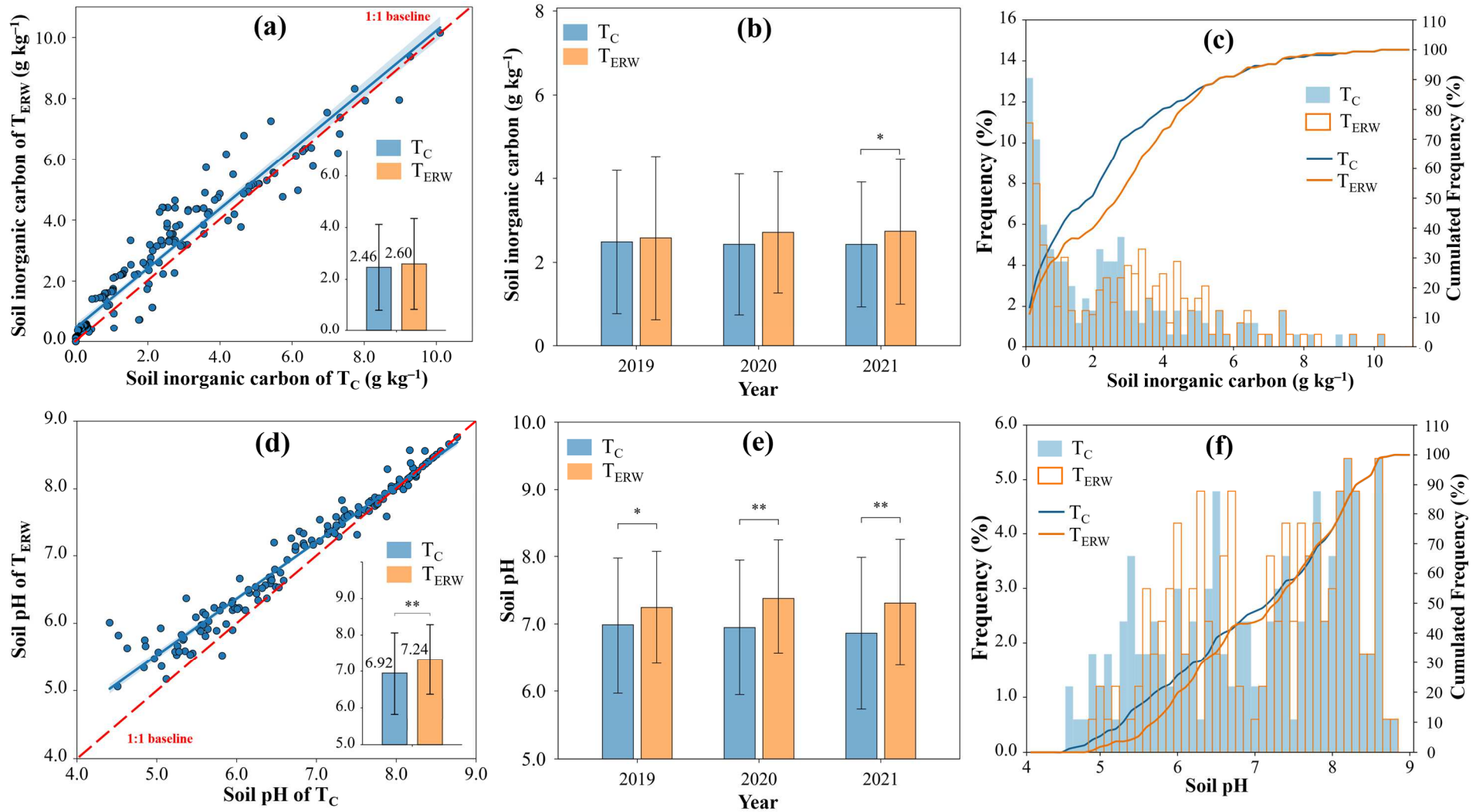


Fig. 3. The significance comparison (a, d), annual change (b, e) and frequency distribution (c, f) of soil inorganic carbon (a, b) and pH (c, d) in response to enhanced rock weathering. T_C and T_{ERW} is control and enhanced rock weathering treatment. The interior bar plot is a significant comparison in subfigure a and d, and bars show frequency and lines denote cumulated frequency in subfigure c and f. * denote $p < 0.05$, ** is $p < 0.01$, and *** represent $p < 0.001$.

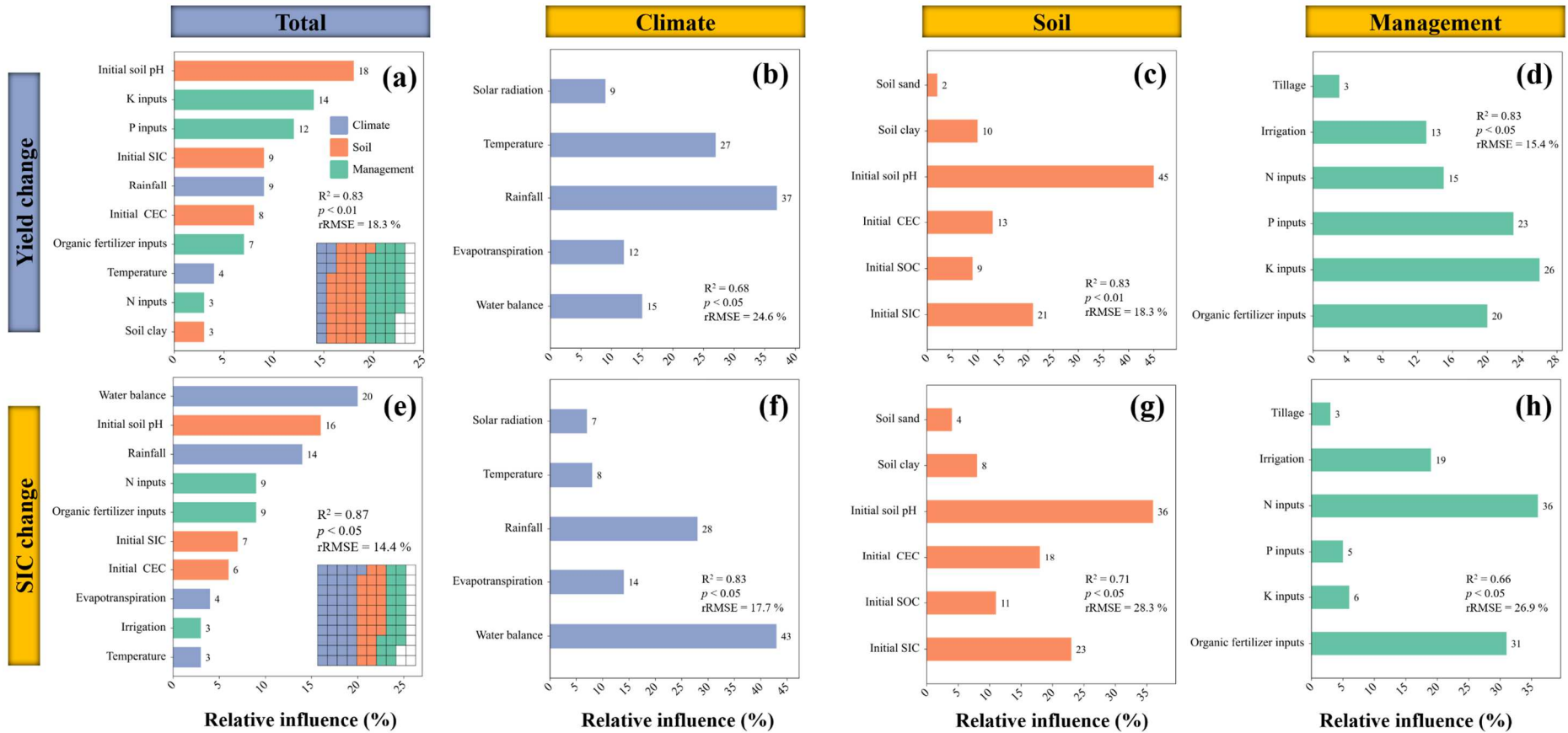


Fig. 4. Relative influence of climate, soil and management drivers to the changes of yield (a, b, c, d) and soil inorganic carbon (e, f, g, h) caused by enhanced rock weathering. Waffle plot show the total contribution of each type of factors, where one square represents 1%.

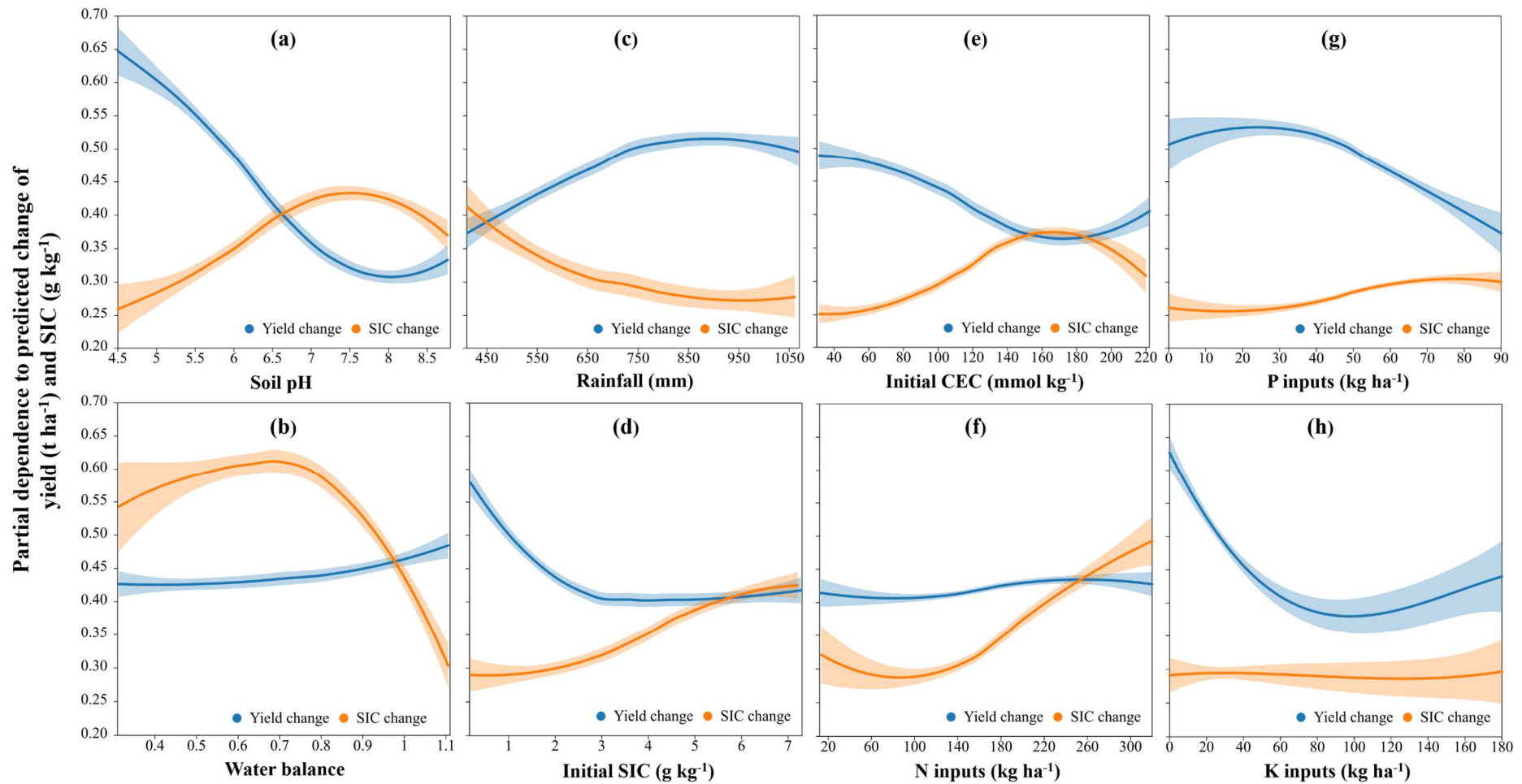


Fig. 5. Partial dependence plots of environment drivers on the changes of yield and soil inorganic carbon. Partial dependence regression curves were locally weighted smoothed and shaded areas indicate the 95% confidence interval.

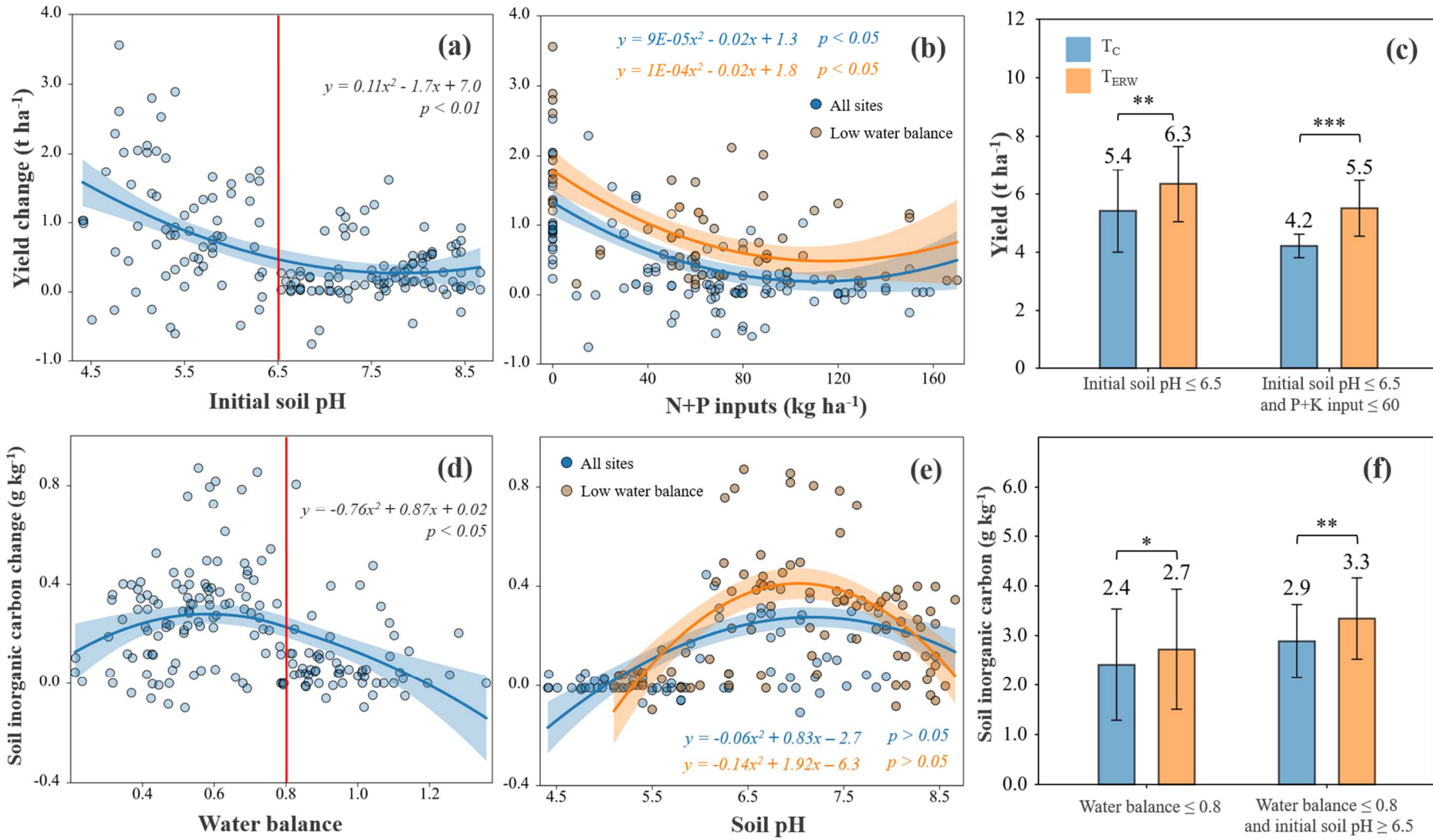


Fig. 6. Effects of initial soil pH, nutrients inputs and water balance on yield (a, b) and soil inorganic carbon changes (d, e), and the yield (c) and soil inorganic carbon (f) comparison between control treatment (T_C) and enhanced rock weathering treatment (T_{ERW}). * denote $p < 0.05$, ** is $p < 0.01$ and *** represent $p < 0.001$.

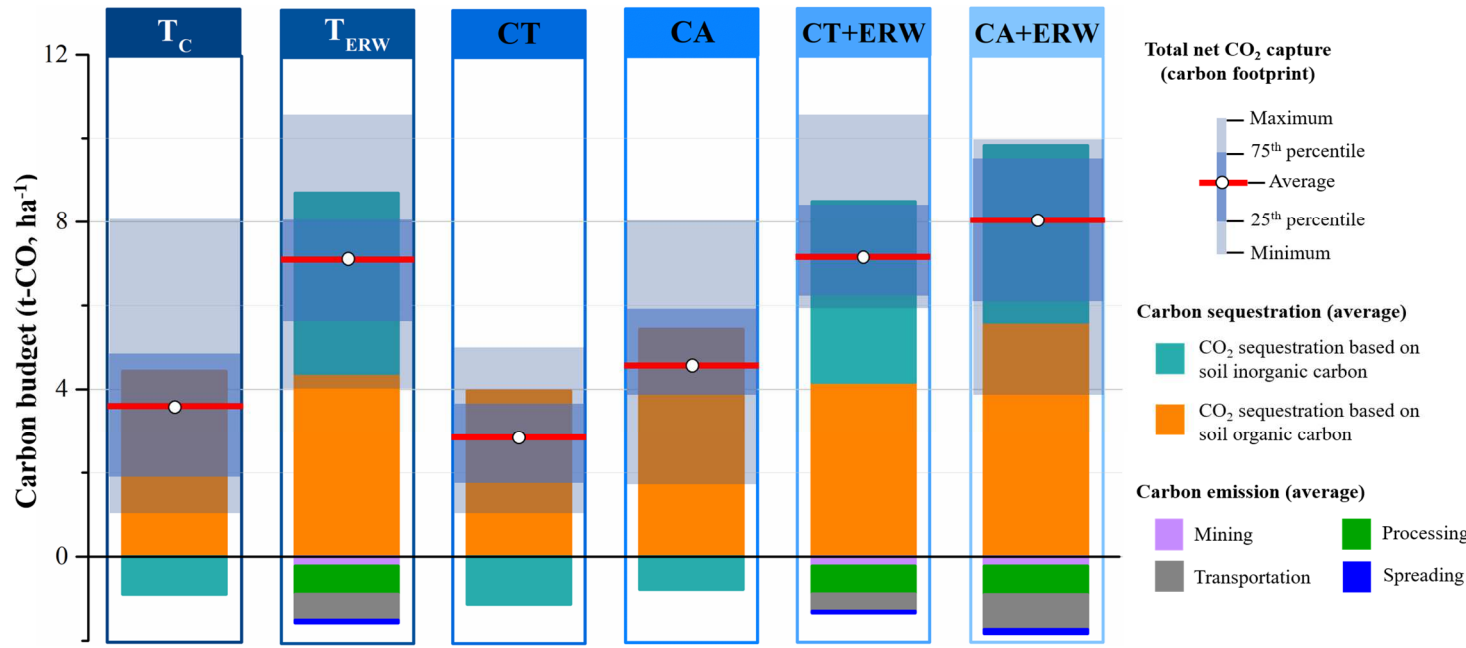
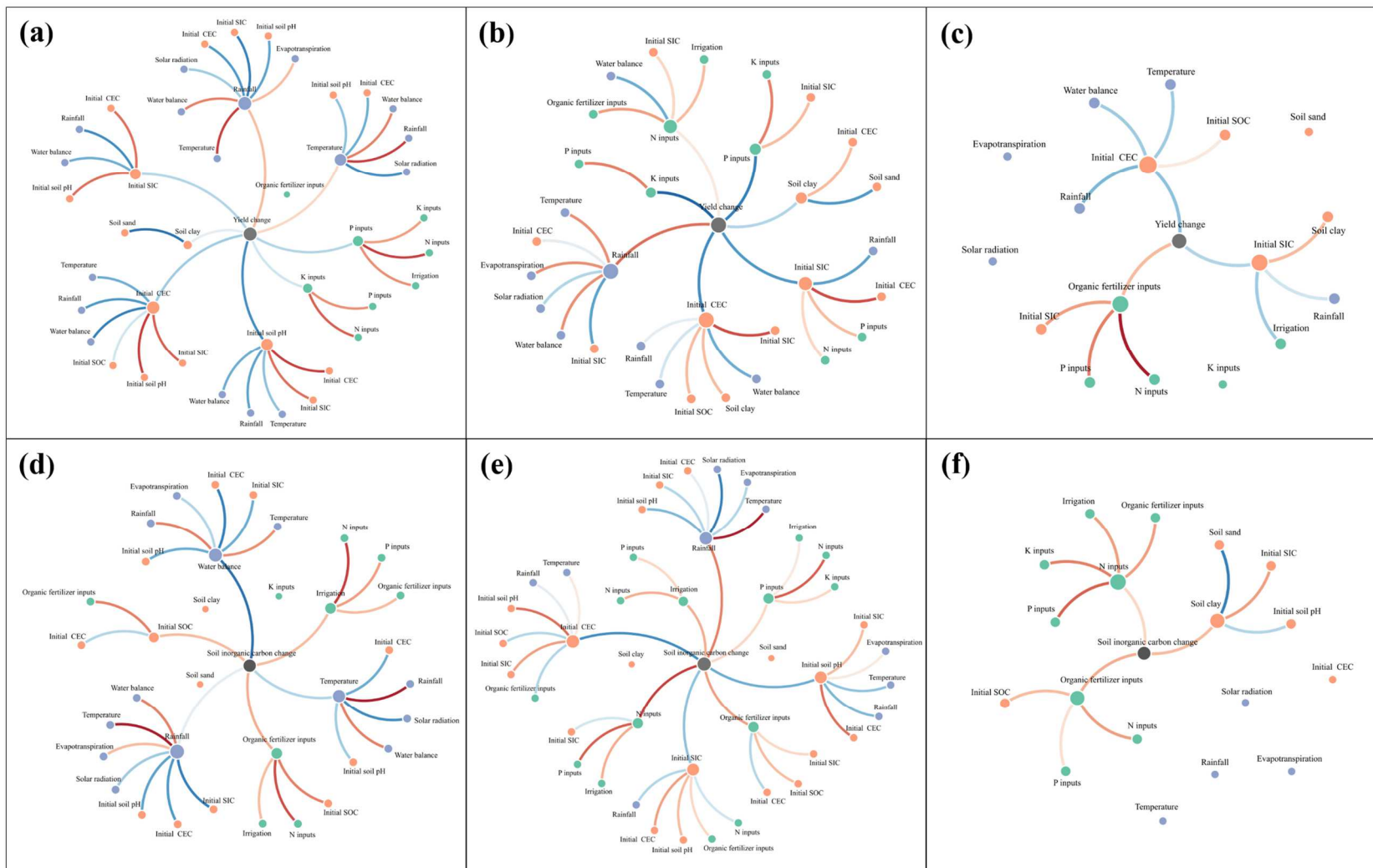


Fig. 7. Carbon budget in the low water balance region (≤ 0.8) from 2019 to 2022. T_c is control treatment, T_{ERW} is enhanced rock weathering treatment, CT denotes conventional tillage system, and CA represents conservation agriculture system.



Variable types

- Climate
- Soil
- Management
- indicator

Correlation coefficient

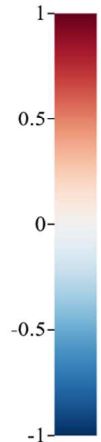


Fig. 8. Correlation coefficient network to analyze the different pathways link environment drivers to the change of yield and soil inorganic carbon by enhanced rock weathering. a-c are yield changes in all regions, low initial soil pH (≤ 6.5) and initial high pH (> 6.5) sites, and d-f are soil inorganic carbon changes in all regions, low-water balance (≤ 0.8) and high-water balance (> 0.8) sites. Different node colors represent variable types, and different line colors represent the magnitude of the correlation coefficient.

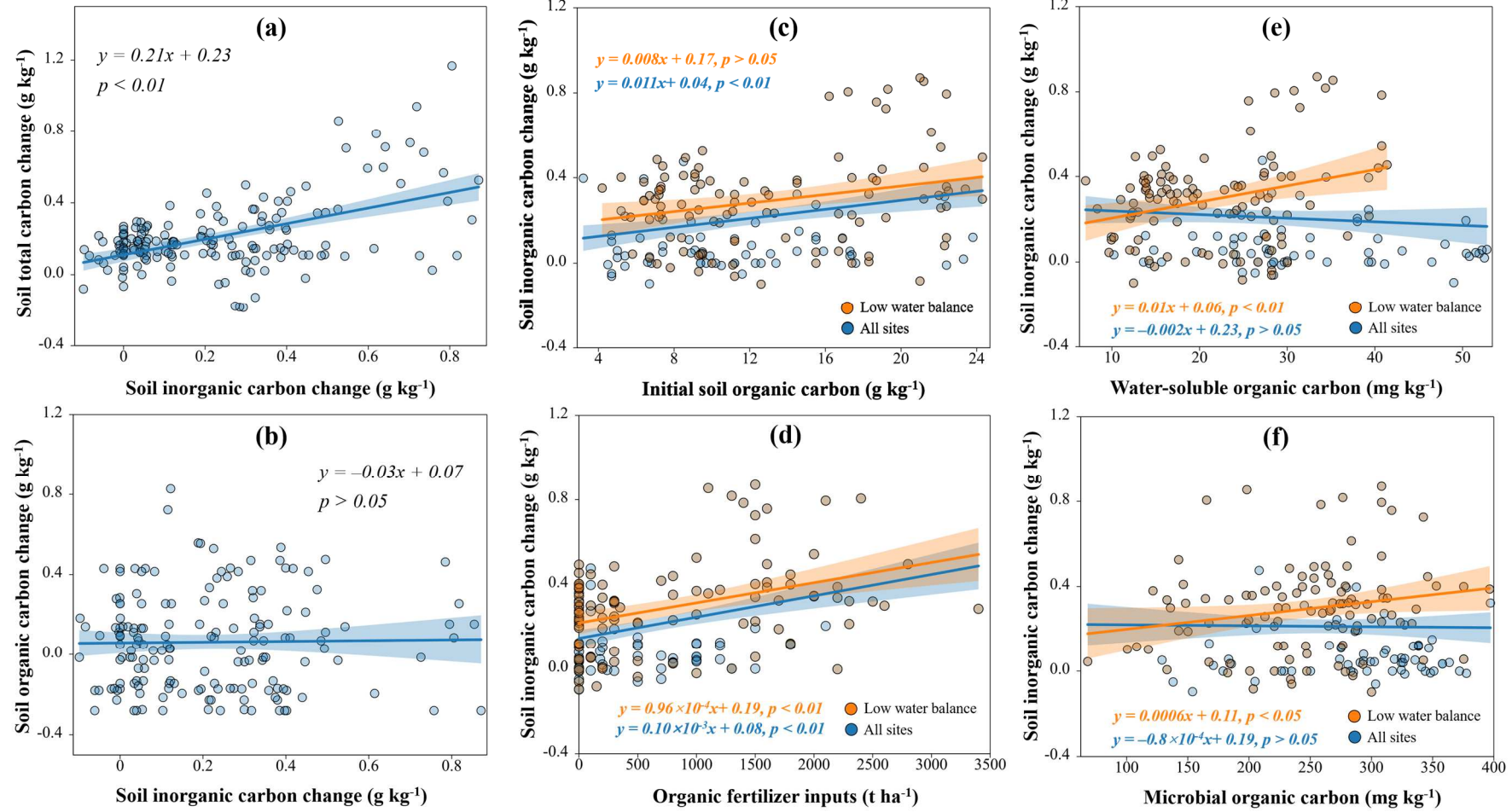


Fig. 9. Relationship between soil total carbon change (a), organic carbon change (b), initial soil organic (c), organic fertilizer input (d), water-soluble organic carbon (e) and microbial organic carbon (f) and SIC changes induced by enhanced rock weathering. Low water balance denotes the sites of water balance coefficient ≤ 0.8 .

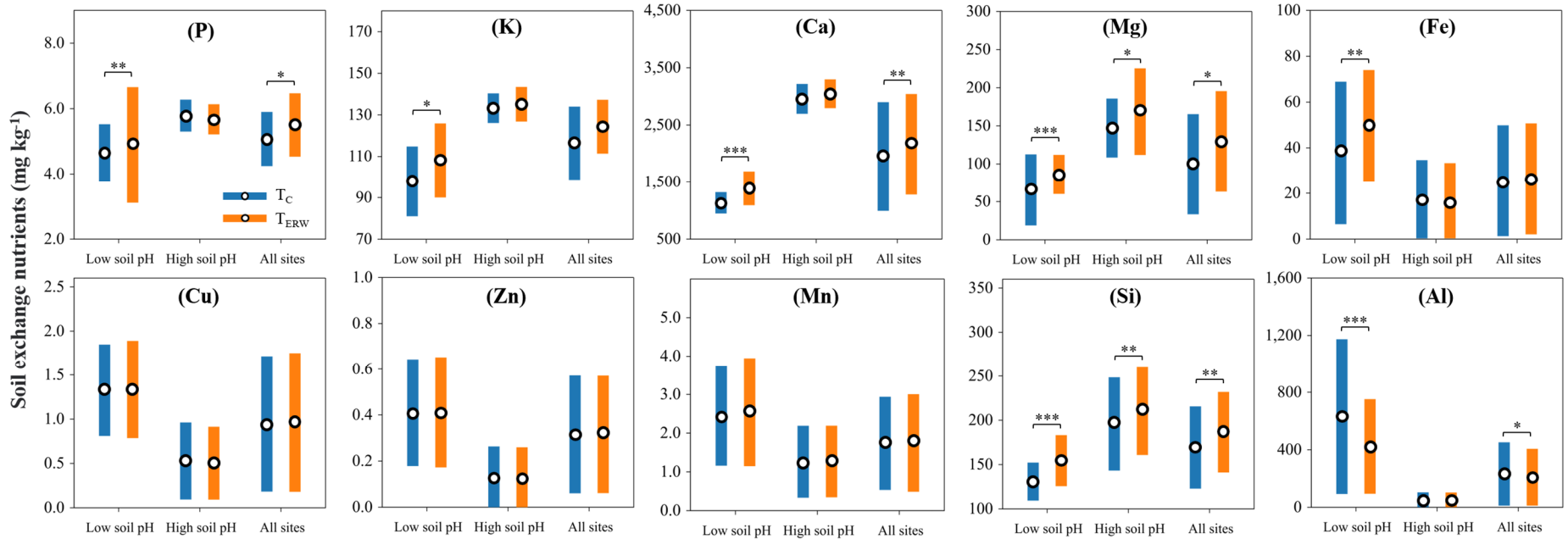


Fig. 10. Comparison of control treatment (T_C) and enhanced rock weathering treatment (T_{ERW}) on the soil exchange nutrients. Dots are the average, and error bars are the standard deviation. Low soil pH denotes the sites of initial soil pH ≤ 6.5 , and high soil pH is the sites of initial soil pH > 6.5 . A result with an asterisk represents a significant difference between T_C and T_{ERW}, and * denote $p < 0.05$, ** is $p < 0.01$ and *** represent $p < 0.001$.

Table 1

List of field monitoring and environment driver variables

Type	Variable	Unit	Number ¹	Data source
Field monitoring data	Yield	t ha ⁻¹	103 (57) ²	
	Biomass	t ha ⁻¹	103 (57)	
	Soil inorganic carbon	g kg ⁻¹	138	
	Soil pH		138	Comparison of T _C and T _{ERW} by sampling and measurement
	Soil exchangeable nutrients (P, K, Ca, Mg, Fe, Mn, Cu, Zn, Si) and exchangeable Al	mg kg ⁻¹	138	
	Solar radiation ³	MJ m ⁻²	138	
Climate driver	Mean air temperature	°C	138	County-level annual average through data collection
	Rainfall	mm	138	
	Evapotranspiration	mm	138	Calculated by FAO-PM model
	Water balance		138	The ratio of rainfall to evapotranspiration
	Soil sand	%	138	
Environment driver data	Soil clay	%	138	
	Initial soil pH		138	
	Initial CEC	mmol kg ⁻¹	138	Acquisition and determination of initial soil
	Initial SIC	g kg ⁻¹	138	
	Initial SOC	g kg ⁻¹	138	
Management driver	Tillage method	Conventional tillage = 0 No or reduce tillage = 1	138	
	N input	kg ha ⁻¹	138	
	P input	kg ha ⁻¹	138	Field survey
	K input	kg ha ⁻¹	138	
	Organic fertilizer input	kg ha ⁻¹	138	
	Irrigation	mm	138	

Note: 1. Final sample size after data curation.

2. “Corn yield (winter wheat yield)”, the corn yield was less than 138 because of fallow and rotation.

3. The sunshine hours were converted to solar radiation by Ängström–Prescott equation.

